

CP-violation in the Weinberg 3HDM potential

O. M. Ogreid,^{a,1} P. Osland,^{b,2} and M. N. Rebelo^{c,3}

^aWestern Norway University of Applied Sciences,
Postboks 7030, N-5020 Bergen, Norway,

^bDepartment of Physics and Technology, University of Bergen,
Postboks 7803, N-5020 Bergen, Norway,

^cCentro de Física Teórica de Partículas – CFTP and Dept de Física
Instituto Superior Técnico – IST, Universidade de Lisboa, Av. Rovisco Pais,
P-1049-001 Lisboa, Portugal

Abstract

We explore the phenomenology of Weinberg's $\mathbb{Z}_2 \times \mathbb{Z}_2$ symmetric three-Higgs-doublet potential, allowing for spontaneous violation of CP due to complex vacuum expectation values. An overview of all possible ways of satisfying the stationary-point conditions is given, with one, two or three non-vanishing vacuum expectation values, together with conditions for CP conservation in terms of basis invariants. All possible ways of satisfying the conditions for CP conservation are given. Scans of allowed parameter regions are given, together with measures of CP violation, in terms of the invariants. The light states identified in an earlier paper are further explored in terms of their CP-violating couplings. Loop-induced CP violation in WWZ couplings, as well as charge-asymmetric scattering are also commented on.

¹E-mail: omo@hvl.no

²E-mail: Per.Osland@uib.no

³E-mail: rebelo@tecnico.ulisboa.pt

1 Introduction

Like any three-Higgs-doublet potential, the Weinberg 3HDM potential [1] has five neutral scalars and two pairs of charged ones. In a recent paper [2] we explored this potential, showing that if we require the existence of an SM-like state, h_{SM} (based on the couplings to WW and ZZ), then the potential tends to yield one or two neutral states below $m_{\text{SM}} = 125$ GeV. This is caused by the fact that by breaking the $\mathbb{Z}_2 \times \mathbb{Z}_2$ symmetry, one also breaks a $U(1) \times U(1)$ symmetry, which is more restrictive than that of the Weinberg potential, and in parameter space is located close to the $\mathbb{Z}_2 \times \mathbb{Z}_2$ symmetry.

While complex vacuum expectation values (vevs) of fields in the potential generally lead to CP violation, there are exceptions. We are identifying these by first establishing a set of basis-invariant quantities, having the property that if any one of them is non-zero, then CP is violated by the vacuum. Next, we identify every solution, for which all these invariants simultaneously vanish, and CP is conserved. Some of these cases allow for complex vevs.

Here, we also further explore the CP-violating aspects of the potential, based on a parameter scan. After imposing the more important theoretical constraints, we also impose the more important experimental constraints, namely those due to the electroweak precision observables (S , T , U), $h_{\text{SM}} \rightarrow \gamma\gamma$, $\bar{B} \rightarrow X_s \gamma$ and the electron electric dipole moment (EDM).

Any 3HDM potential has two pairs of charged scalars. When the CP symmetry is broken, as is the case here, there will be CP-violating processes in the scalar sector (not involving couplings to fermions), most easily illustrated in the charged-scalar sector.

With the neutral states labelled h_1 , h_2 , h_3 , h_4 and h_5 (with increasing masses), we saw that the constraints imposed [2, 3] led to h_2 or h_3 predominantly being identified as the SM candidate. In the present paper we therefore focus on these two cases.

This paper is organized as follows. In section 2 we define our notation, then, in section 3 we present an overview of different ways of satisfying the stationary-point equations, identifying a minimum that may be new to the literature. This solution conserves a \mathbb{Z}_2 symmetry, while violating CP. In section 4 we present invariants that must vanish for CP to be conserved. Then, in section 5 we give an overview of possible Yukawa structures. Section 6 presents an overview of the most relevant experimental constraints, those due to the electroweak precision observables, the di-gamma signal strength, $\bar{B} \rightarrow X_s \gamma$ and the electron EDM. In section 7 we review the impact the constraints have on the CP-violating invariants, and in section 8 we discuss more exotic CP-violating processes. Results, in terms of allowed parameter space, are given in section 9, and concluding remarks in section 10. Transformations to the Higgs basis are presented in appendix A, and special cases of CP conservation are presented in appendix B.

2 Notation and definitions

We parametrize the three Higgs doublets after electroweak symmetry breaking as

$$\phi_i = e^{i\theta_i} \begin{pmatrix} \varphi_i^+ \\ \frac{1}{\sqrt{2}}(v_i + \eta_i + i\chi_i) \end{pmatrix}, \quad i = 1, 2, 3. \quad (2.1)$$

Here, the v_i are real. Imposing two \mathbb{Z}_2 symmetries, we automatically get a third one, due to the overall hermiticity of the potential. The doublets may then be assigned the $\mathbb{Z}_2 \times \mathbb{Z}_2 \times \mathbb{Z}_2$ parities

$$\phi_1 : (+1, +1, -1) \quad \phi_2 : (-1, +1, +1) \quad \phi_3 : (+1, -1, +1). \quad (2.2)$$

In this basis, which we will refer to as the symmetry basis, we write the most general $\mathbb{Z}_2 \times \mathbb{Z}_2$ -symmetric potential [1], following the notation of Ivanov and Nishi [4]¹,

$$\begin{aligned} V = & -[m_{11}(\phi_1^\dagger \phi_1) + m_{22}(\phi_2^\dagger \phi_2) + m_{33}(\phi_3^\dagger \phi_3)] + \lambda_{11}(\phi_1^\dagger \phi_1)^2 + \lambda_{22}(\phi_2^\dagger \phi_2)^2 + \lambda_{33}(\phi_3^\dagger \phi_3)^2 \\ & + \lambda_{12}(\phi_1^\dagger \phi_1)(\phi_2^\dagger \phi_2) + \lambda_{13}(\phi_1^\dagger \phi_1)(\phi_3^\dagger \phi_3) + \lambda_{23}(\phi_2^\dagger \phi_2)(\phi_3^\dagger \phi_3) \\ & + \lambda'_{12}(\phi_1^\dagger \phi_2)(\phi_2^\dagger \phi_1) + \lambda'_{13}(\phi_1^\dagger \phi_3)(\phi_3^\dagger \phi_1) + \lambda'_{23}(\phi_2^\dagger \phi_3)(\phi_3^\dagger \phi_2) \\ & + \lambda_1[(\phi_2^\dagger \phi_3)^2 + (\phi_3^\dagger \phi_2)^2] + \lambda_2[(\phi_3^\dagger \phi_1)^2 + (\phi_1^\dagger \phi_3)^2] + \lambda_3[(\phi_1^\dagger \phi_2)^2 + (\phi_2^\dagger \phi_1)^2]. \end{aligned} \quad (2.3)$$

We shall assume real coefficients (i.e., we consider a CP-invariant potential), but allow for spontaneous CP violation via complex vevs [5] as discussed in Ref. [2].

The physical fields, h_i and h_k^+ , will be related to those of Eq. (2.1) via the rotation matrices \mathcal{O} and \mathcal{U} by

$$h_i \equiv \sum_{m=1}^6 \mathcal{O}_{im} \varphi_m, \quad h_k^+ \equiv \sum_{n=1}^3 \mathcal{U}_{kn} \varphi_n^+, \quad (2.4)$$

where $\varphi_m = (\eta_1, \eta_2, \eta_3, \chi_1, \chi_2, \chi_3)$. Here, $h_0 = G^0$ and $h_0^+ = G^+$ are the Goldstone bosons, \mathcal{O} is orthogonal and \mathcal{U} is unitary. The corresponding relations for the mixing matrices in the Higgs basis are given in Appendix A.

The $U(1) \times U(1)$ limit alluded to above, is obtained by setting $\lambda_1 = \lambda_2 = \lambda_3 = 0$. In that limit, with non-vanishing vevs breaking the symmetry, there are two massless states. For small, but nonzero values of λ_1 , λ_2 and λ_3 the low-mass states which were the focus of our earlier work, may be considered analytic “continuations” of those massless ones.

3 Solutions of stationary-point equations

Let $\{i, j, k\}$ be any permutation of $\{1, 2, 3\}$. We shall in the following interpret $\lambda_{ij} = \lambda_{ji}$ and $\lambda'_{ij} = \lambda'_{ji}$ whenever $i > j$. Here, we shall (for symmetry reasons) assume the most general form of the vevs, i.e.

$$\phi_i = \frac{e^{i\theta_i}}{\sqrt{2}} \begin{pmatrix} 0 \\ v_i \end{pmatrix}, \quad i = 1, 2, 3. \quad (3.1)$$

¹Following tradition, we shall refer to the potential as being $\mathbb{Z}_2 \times \mathbb{Z}_2$ symmetric.

Below, we list all solutions of the stationary-point equations for the real potential, indicating whether they conserve (CPC) or violate CP (CPV).

Solution 1 (CPC):

$$v_i = 0, \quad v_j = 0, \quad m_{kk} = \lambda_{kk} v_k^2. \quad (3.2)$$

Solution 2 (CPV):

$$v_i = 0, \quad \lambda_i = 0, \\ m_{jj} = \frac{1}{2} v_k^2 (\lambda'_{jk} + \lambda_{jk}) + \lambda_{jj} v_j^2, \quad m_{kk} = \frac{1}{2} v_j^2 (\lambda'_{jk} + \lambda_{jk}) + \lambda_{kk} v_k^2. \quad (3.3)$$

This solution has a \mathbb{Z}_2 symmetry preserved by the vacuum.

Solution 3 (CPC):

$$v_i = 0, \quad \sin(\theta_k - \theta_j) = 0, \\ m_{jj} = \frac{1}{2} v_k^2 (\lambda'_{jk} + \lambda_{jk} + 2\lambda_i) + \lambda_{jj} v_j^2, \quad m_{kk} = \frac{1}{2} v_j^2 (\lambda'_{jk} + \lambda_{jk} + 2\lambda_i) + \lambda_{kk} v_k^2. \quad (3.4)$$

Solution 4 (CPC):

$$v_i = 0, \quad \cos(\theta_k - \theta_j) = 0, \\ m_{jj} = \frac{1}{2} v_k^2 (\lambda'_{jk} + \lambda_{jk} - 2\lambda_i) + \lambda_{jj} v_j^2, \quad m_{kk} = \frac{1}{2} v_j^2 (\lambda'_{jk} + \lambda_{jk} - 2\lambda_i) + \lambda_{kk} v_k^2. \quad (3.5)$$

Solution 5 (CPC):

$$\sin(\theta_3 - \theta_1) = \sin(\theta_2 - \theta_1) = 0, \\ m_{11} = \frac{1}{2} (v_2^2 (\lambda'_{12} + 2\lambda_3 + \lambda_{12}) + v_3^2 (\lambda'_{13} + 2\lambda_2 + \lambda_{13}) + 2\lambda_{11} v_1^2), \\ m_{22} = \frac{1}{2} (v_1^2 (\lambda'_{12} + 2\lambda_3 + \lambda_{12}) + v_3^2 (\lambda'_{23} + 2\lambda_1 + \lambda_{23}) + 2\lambda_{22} v_2^2), \\ m_{33} = \frac{1}{2} (v_1^2 (\lambda'_{13} + 2\lambda_2 + \lambda_{13}) + v_2^2 (\lambda'_{23} + 2\lambda_1 + \lambda_{23}) + 2\lambda_{33} v_3^2). \quad (3.6)$$

Solution 6 (CPC):

$$\cos(\theta_3 - \theta_1) = \sin(\theta_2 - \theta_1) = 0, \\ m_{11} = \frac{1}{2} (v_2^2 (\lambda'_{12} + 2\lambda_3 + \lambda_{12}) + v_3^2 (\lambda'_{13} - 2\lambda_2 + \lambda_{13}) + 2\lambda_{11} v_1^2), \\ m_{22} = \frac{1}{2} (v_1^2 (\lambda'_{12} + 2\lambda_3 + \lambda_{12}) + v_3^2 (\lambda'_{23} - 2\lambda_1 + \lambda_{23}) + 2\lambda_{22} v_2^2), \\ m_{33} = \frac{1}{2} (v_1^2 (\lambda'_{13} - 2\lambda_2 + \lambda_{13}) + v_2^2 (\lambda'_{23} - 2\lambda_1 + \lambda_{23}) + 2\lambda_{33} v_3^2). \quad (3.7)$$

Solution 7 (CPC):

$$\sin(\theta_3 - \theta_1) = \cos(\theta_2 - \theta_1) = 0, \\ m_{11} = \frac{1}{2} (v_2^2 (\lambda'_{12} - 2\lambda_3 + \lambda_{12}) + v_3^2 (\lambda'_{13} + 2\lambda_2 + \lambda_{13}) + 2\lambda_{11} v_1^2), \\ m_{22} = \frac{1}{2} (v_1^2 (\lambda'_{12} - 2\lambda_3 + \lambda_{12}) + v_3^2 (\lambda'_{23} - 2\lambda_1 + \lambda_{23}) + 2\lambda_{22} v_2^2), \\ m_{33} = \frac{1}{2} (v_1^2 (\lambda'_{13} + 2\lambda_2 + \lambda_{13}) + v_2^2 (\lambda'_{23} - 2\lambda_1 + \lambda_{23}) + 2\lambda_{33} v_3^2). \quad (3.8)$$

Solution 8 (CPC):

$$\cos(\theta_3 - \theta_1) = \cos(\theta_2 - \theta_1) = 0, \\ m_{11} = \frac{1}{2} (v_2^2 (\lambda'_{12} - 2\lambda_3 + \lambda_{12}) + v_3^2 (\lambda'_{13} - 2\lambda_2 + \lambda_{13}) + 2\lambda_{11} v_1^2),$$

$$\begin{aligned}
m_{22} &= \frac{1}{2} (v_1^2 (\lambda'_{12} - 2\lambda_3 + \lambda_{12}) + v_3^2 (\lambda'_{23} + 2\lambda_1 + \lambda_{23}) + 2\lambda_{22}v_2^2), \\
m_{33} &= \frac{1}{2} (v_1^2 (\lambda'_{13} - 2\lambda_2 + \lambda_{13}) + v_2^2 (\lambda'_{23} + 2\lambda_1 + \lambda_{23}) + 2\lambda_{33}v_3^2).
\end{aligned} \tag{3.9}$$

Solution 9 (CPC):

$$\begin{aligned}
\sin(\theta_j - \theta_i) &= 0, \quad \lambda_i = \lambda_j = 0, \\
m_{ii} &= \frac{1}{2} (v_j^2 (\lambda'_{ij} + \lambda_{ij} + 2\lambda_k) + v_k^2 (\lambda'_{ik} + \lambda_{ik}) + 2\lambda_{ii}v_i^2), \\
m_{jj} &= \frac{1}{2} (v_i^2 (\lambda'_{ij} + \lambda_{ij} + 2\lambda_k) + v_k^2 (\lambda'_{jk} + \lambda_{jk}) + 2\lambda_{jj}v_j^2), \\
m_{kk} &= \frac{1}{2} (v_i^2 (\lambda'_{ik} + \lambda_{ik}) + v_j^2 (\lambda'_{jk} + \lambda_{jk}) + 2\lambda_{kk}v_k^2).
\end{aligned} \tag{3.10}$$

Solution 10 (CPC):

$$\begin{aligned}
\cos(\theta_j - \theta_i) &= 0, \quad \lambda_i = \lambda_j = 0, \\
m_{ii} &= \frac{1}{2} (v_j^2 (\lambda'_{ij} + \lambda_{ij} - 2\lambda_k) + v_k^2 (\lambda'_{ik} + \lambda_{ik}) + 2\lambda_{ii}v_i^2), \\
m_{jj} &= \frac{1}{2} (v_i^2 (\lambda'_{ij} + \lambda_{ij} - 2\lambda_k) + v_k^2 (\lambda'_{jk} + \lambda_{jk}) + 2\lambda_{jj}v_j^2), \\
m_{kk} &= \frac{1}{2} (v_i^2 (\lambda'_{ik} + \lambda_{ik}) + v_j^2 (\lambda'_{jk} + \lambda_{jk}) + 2\lambda_{kk}v_k^2).
\end{aligned} \tag{3.11}$$

Solution 11 (CPV):

$$\begin{aligned}
m_{11} &= \frac{1}{2} \left(v_2^2 (\lambda'_{12} + \lambda_{12}) + v_3^2 (\lambda'_{13} + \lambda_{13}) + \frac{2\lambda_1 v_2^2 v_3^2 \sin^2 2(\theta_2 - \theta_3)}{v_1^2 \sin 2(\theta_1 - \theta_2) \sin 2(\theta_1 - \theta_3)} + 2\lambda_{11}v_1^2 \right), \\
m_{22} &= \frac{1}{2} (v_1^2 (\lambda'_{12} + \lambda_{12}) + v_3^2 (\lambda'_{23} + \lambda_{23}) + 2\lambda_{22}v_2^2) + \lambda_1 v_3^2 \frac{\sin 2(\theta_1 - \theta_3)}{\sin 2(\theta_1 - \theta_2)}, \\
m_{33} &= \frac{1}{2} (v_1^2 (\lambda'_{13} + \lambda_{13}) + v_2^2 (\lambda'_{23} + \lambda_{23}) + 2\lambda_{33}v_3^2) + \lambda_1 v_2^2 \frac{\sin 2(\theta_1 - \theta_2)}{\sin 2(\theta_1 - \theta_3)}, \\
\lambda_3 &= \frac{\lambda_1 v_3^2 \sin 2(\theta_2 - \theta_3)}{v_1^2 \sin 2(\theta_1 - \theta_2)}, \quad \lambda_2 = -\frac{\lambda_1 v_2^2 \sin 2(\theta_2 - \theta_3)}{v_1^2 \sin 2(\theta_1 - \theta_3)}.
\end{aligned} \tag{3.12}$$

The latter is the solution identified by Branco [5] and studied in our earlier work [2, 3], as well as in the bulk of the present paper.

One can understand the existence of the two types of solutions that allow for spontaneous CP violation by looking at the scalar potential given by Eq. (2.3). Spontaneous CP violation can only occur if there are complex vevs. In the case of $\lambda_i = 0$ and $v_i = 0$ (for a single i) there is only one relative phase in the vacuum which gives rise to a complex λ_j in the basis where all vevs are real. The minimisation conditions for the vacuum phases in this case are trivially satisfied and therefore do not impose any additional constraints on the λ s, this is Solution 2. The most general case with all $\lambda_k \neq 0$ and a general complex vacuum corresponds to Solution 11 where the minimisation conditions for the two independent vacuum phases lead to the possibility of expressing λ_i and λ_j in terms of λ_k and vevs.

4 Conditions for CP conservation

With complex vevs, the potential will in general violate CP. However, there are special cases in which CP is conserved. These can be identified from the study of CP-odd invariants.

When they all vanish, CP is conserved. The invariants are expressed in terms of the tensors Z , Y and \hat{V} , where Z and Y are defined by the expansion [6] (see also Refs. [7–13])

$$V = Y_{ab}(\phi_a^\dagger \phi_b) + \frac{1}{2} Z_{abcd}(\phi_a^\dagger \phi_b)(\phi_c^\dagger \phi_d), \quad (4.1)$$

whereas the vacuum is represented by \hat{V} ,

$$\hat{V}_{ab} = \frac{v_a e^{i\theta_a}}{v} \frac{v_b e^{-i\theta_b}}{v}. \quad (4.2)$$

In terms of this notation, we can state the following

Theorem:

Whenever the stationary-point equations are satisfied, the real $\mathbb{Z}_2 \times \mathbb{Z}_2$ -symmetric three-Higgs-doublet potential conserves CP if and only if the following 15 CP-odd invariants all vanish:

$$J_1 = \text{Im} \{ \hat{V}_{ac} \hat{V}_{be} Z_{cadf} Z_{edfg} Z_{gbhh} \}, \quad (4.3a)$$

$$J_2 = \text{Im} \{ \hat{V}_{ac} \hat{V}_{be} Z_{cadf} Z_{edfg} Z_{ghhb} \}, \quad (4.3b)$$

$$J_3 = \text{Im} \{ \hat{V}_{ac} \hat{V}_{be} Z_{cadf} Z_{egfd} Z_{gbhh} \}, \quad (4.3c)$$

$$J_4 = \text{Im} \{ \hat{V}_{ac} \hat{V}_{bd} Z_{cedg} Z_{eafh} Z_{gbhf} \}, \quad (4.3d)$$

$$J_5 = \text{Im} \{ \hat{V}_{ac} \hat{V}_{bd} Z_{cedg} Z_{ehfa} Z_{gfhb} \}, \quad (4.3e)$$

$$J_6 = \text{Im} \{ \hat{V}_{ac} \hat{V}_{bd} Z_{cedf} Z_{eafg} Z_{gbhh} \}, \quad (4.3f)$$

$$J_7 = \text{Im} \{ \hat{V}_{ad} \hat{V}_{be} \hat{V}_{cf} Z_{daeh} Z_{fbgi} Z_{hcig} \}, \quad (4.3g)$$

$$J_8 = \text{Im} \{ \hat{V}_{ad} \hat{V}_{be} \hat{V}_{cf} Z_{daeh} Z_{figb} Z_{hgic} \}, \quad (4.3h)$$

$$J_9 = \text{Im} \{ \hat{V}_{ad} \hat{V}_{be} \hat{V}_{cf} Z_{daeg} Z_{fbgh} Z_{hcii} \}, \quad (4.3i)$$

$$J_{10} = \text{Im} \{ \hat{V}_{ad} \hat{V}_{be} \hat{V}_{cf} Z_{daeg} Z_{fhgi} Z_{hbic} \}, \quad (4.3j)$$

$$J_{11} = \text{Im} \{ \hat{V}_{ac} \hat{V}_{be} Z_{cadg} Z_{edff} Z_{gihh} Z_{ibjj} \}, \quad (4.3k)$$

$$J_{12} = \text{Im} \{ \hat{V}_{ac} \hat{V}_{be} Z_{cadg} Z_{effd} Z_{ghhi} Z_{ijjb} \}, \quad (4.3l)$$

$$J_{13} = \text{Im} \{ \hat{V}_{ac} \hat{V}_{be} Z_{cadf} Z_{edfg} Z_{gihj} Z_{ibjh} \}, \quad (4.3m)$$

$$J_{14} = \text{Im} \{ \hat{V}_{ac} \hat{V}_{bd} Z_{cedf} Z_{eafg} Z_{gihj} Z_{ibjh} \}, \quad (4.3n)$$

$$v^6 J_{15} = \text{Im} \{ \hat{V}_{ac} \hat{V}_{bd} Y_{cf} Y_{dg} Y_{ea} Z_{fbge} \}. \quad (4.3o)$$

The following remarks are important:

1. This result relies on the fact that the stationary-point equations are all satisfied (in other words: after electroweak symmetry breaking has taken place). There are several ways to solve the stationary-point equations (see section 3). The above result is valid for all possible ways they can be solved.

2. There are no redundant invariants in the set of 15 invariants listed. For each invariant J_i , we have located a point in parameter-space where $J_i \neq 0$ while the remaining 14 invariants vanish.
3. One could imagine picking a set of CP-odd invariants different from the one presented here, whose simultaneous vanishing would be equivalent to the model being CP-conserving. We do not know if there could exist such a set where the total number of invariants is less than 15.
4. Although we have proven that the vanishing of the 15 CP-odd invariants J_i is equivalent to having a CP conserving model, that does not mean that any CP-odd quantity can be written as a linear combination of the 15 J_i . This is also known from the 2HDM, where $\text{Im } J_1 = \text{Im } J_2 = \text{Im } J_{30} = 0$ is equivalent to having a CP conserving 2HDM [14]. Yet, in the 2HDM, it is not possible to write all CP-odd quantities as linear combinations of those three CP-odd invariants. Therefore, in [14], the authors introduced additional CP-odd invariants in their eqs. (4.6) and (4.14). Those additional invariants vanish simultaneously with the three CP-odd invariants that guarantee a CP-conserving model, yet they are redundant in order to guarantee CP conservation, but they were introduced in order to express the CP-odd quantities studied there in terms of CP-odd invariants. In a later work [15], the same authors were able to express all CP-odd quantities as linear combinations just by adding one extra invariant $\text{Im } J_{11}$ to the set of the original three CP-odd invariants.

This can be understood as follows. The vanishing of $\{\text{Im } J_1, \text{Im } J_2, \text{Im } J_{30}\}$ guarantees a CP-conserving model, but not all CP-odd quantities can be written as linear combinations of these three. The set $\{\text{Im } J_1, \text{Im } J_2, \text{Im } J_{30}, \text{Im } J_{11}\}$ constitutes what may be called a “linear algebraic basis” for CP-odd quantities in the 2HDM, making it possible to write all CP-odd quantities as linear combinations of these four CP-odd invariants. The same thing happens for the model we study here. While the simultaneous vanishing of the 15 J_i is equivalent to CP conservation, we would need additional CP-odd invariants in order to express any CP-odd quantity of the model as a linear combination of CP-odd invariants. We would have to extend the set of the 15 J_i with additional J_i (number unknown) in order to get a “linear algebraic basis” for CP-odd invariants of the model. This is, however, beyond the scope of the present work.

In order to arrive at the result presented in this theorem, we constructed a large amount of CP-odd invariants by contracting indices among \hat{V} -, Y - and Z -tensors. We started by first carefully picking some invariants that were algebraically simple enough so that the equations that resulted from demanding the vanishing of the invariants were possible to solve algebraically. Through a process of trial and error, we carefully added more invariants to the set, until we finally arrived at the set of the 15 above invariants. Demanding the simultaneous vanishing of these 15 invariants, gives us a set of 15 equations,

$$J_i = 0, \quad i = 1, \dots, 15. \quad (4.4)$$

It turns out that it is possible to solve this set of equations algebraically. All possible solutions of this set of equations are presented in appendix B. We ended up with a total of 80 different solutions (counting all possible permutations) to the set of equations. For each of these solutions, we were able to show that the solution implies a CP-conserving model. This was done by explicit construction of a basis change that renders both the parameters of the potential and the vacuum real, implying CP conservation. These basis changes are also presented in appendix B along with the solutions.

In summary, using Mathematica [16], we have shown that the fifteen conditions of Eq. (4.4) are enough to force the potential to be real in a basis where the vevs are also real.

We note that all invariants involve two or three factors \hat{V} , each being a product of a vev with another that is complex conjugated. These invariants also involve coefficients of the potential. As examples, for $\{i, j, k\} \in \{1, 2, 3\}$,

$$J_1 = \frac{-2v_i^2 v_j^2}{v^4} \lambda_k \sin 2(\theta_j - \theta_i) (\lambda_{ij} + \lambda'_{ij}) [2(\lambda_{ii} - \lambda_{jj}) + \lambda_{ik} - \lambda_{jk}] + \text{permutations}, \quad (4.5a)$$

$$J_2 = \frac{-2v_i^2 v_j^2}{v^4} \lambda_k \sin 2(\theta_j - \theta_i) (\lambda_{ij} + \lambda'_{ij}) [2(\lambda_{ii} - \lambda_{jj}) + \lambda'_{ik} - \lambda'_{jk}] + \text{permutations}, \quad (4.5b)$$

$$J_3 = \frac{-4v_i^2 v_j^2}{v^4} \lambda_k \sin 2(\theta_j - \theta_i) \lambda'_{ij} [2(\lambda_{ii} - \lambda_{jj}) + \lambda_{ik} - \lambda_{jk}] + \text{permutations}. \quad (4.5c)$$

For the $\mathbb{Z}_2 \times \mathbb{Z}_2$ -symmetric real potential there are no CP-odd invariants with only *one* \hat{V}_{ac} . This is due to the high degree of symmetry of the potential, as commented on in appendix C.

Whenever there is a CP-violating quantity, such as for instance an asymmetry of the form

$$\mathcal{A}_{\text{ch}} = \frac{\sigma(h_i^+ h_i^- \rightarrow h_2^+ h_1^-) - \sigma(h_i^+ h_i^- \rightarrow h_2^- h_1^+)}{\sigma(h_i^+ h_i^- \rightarrow h_2^+ h_1^-) + \sigma(h_i^+ h_i^- \rightarrow h_2^- h_1^+)}, \quad (4.6)$$

it will be possible to express it in terms of non-vanishing CP-odd invariants like the ones in Eq. (4.3). Even though vanishing of the latter is sufficient to guarantee that CP is conserved, a given CP violating quantity may be directly related to a CP-odd invariant not contained in this set. In the CP-conserving limit all possible CP-odd invariants will vanish simultaneously.

Spontaneous CP violation would show up in processes like this, via interference involving trilinear couplings of charged and neutral scalars, each trilinear vertex proportional to a complex vev.

As global measures of CP violation, we shall explore two quantities based on these invariants,

$$A_{\text{sum}} = \log_{10} \sum_{i=1}^{15} J_i^2, \quad A_{\text{max}} = \log_{10} (\max_i J_i^2). \quad (4.7)$$

CP violation is also possible with only two vevs being non-zero. An example is provided by Solution 2 of section 3,

$$v_1 = 0, \quad \lambda_1 = 0, \quad (4.8a)$$

$$m_{22} = v_2^2 \lambda_{22} + \frac{1}{2} v_3^2 (\lambda_{23} + \lambda'_{23}), \quad (4.8b)$$

$$m_{33} = v_3^2 \lambda_{33} + \frac{1}{2} v_2^2 (\lambda_{23} + \lambda'_{23}). \quad (4.8c)$$

In this case, we find five non-vanishing invariants. These all contain the factor

$$J_0 \equiv v_2 v_3 \lambda_2 \lambda_3 \sin 2(\theta_2 - \theta_3), \quad (4.9)$$

which would have to be non-zero for CP to be spontaneously violated. In particular, we note that CP violation requires $2(\theta_2 - \theta_3) \neq n\pi$ for n integer. Including non-trivial factors, the non-vanishing invariants are proportional to

$$J_4 \propto J_0 [\lambda'_{12} - \lambda'_{13}], \quad (4.10a)$$

$$J_5 \propto J_0 [\lambda_{12} - \lambda_{13}], \quad (4.10b)$$

$$J_6 \propto J_0 [\lambda_{12} - \lambda_{13} + 2\lambda_{22} - 2\lambda_{33}], \quad (4.10c)$$

$$J_{10} \propto J_0 [2(\lambda_{22} v_2^2 - \lambda_{33} v_3^2) + (\lambda_{23} + \lambda'_{23})(v_3^2 - v_2^2)], \quad (4.10d)$$

$$J_{14} \propto J_0 [\lambda_{12}^2 - \lambda_{13}^2 + \lambda_{12}'^2 - \lambda_{13}'^2 - 4(\lambda_2^2 - \lambda_3^2) + 4(\lambda_{22}^2 - \lambda_{33}^2)]. \quad (4.10e)$$

Actually, this Solution 2 yields a massless state, but that can be avoided by adding a soft symmetry-breaking term and dropping the constraint $\lambda_1 = 0$.

5 Yukawa sector

With three scalar doublets, there are more possible Yukawa structures than in the familiar 2HDM. Table 1 lists all possible Yukawa structures of the $\mathbb{Z}_2 \times \mathbb{Z}_2$ -symmetric 3HDMs that respect Natural Flavour Conservation (NFC). In addition to the \mathbb{Z}_2 -symmetric 2HDM-like structures, this 3HDM allows for a “democratic” structure (often referred to as “Type Z”) where each kind of fermion species (u , d , e) couples to a different doublet. The table does not take into account permutations of indices for different pairs of fields. This permutation symmetry may be broken by the vacuum. With one more doublet, there are also more possibilities for inert doublets.

	u	d	e	Inert doublets
Type I-like	ϕ_1	ϕ_1	ϕ_1	at most 2
Type II-like	ϕ_1	ϕ_2	ϕ_2	at most 1
Lepton specific-like	ϕ_1	ϕ_1	ϕ_2	at most 1
Flipped-like	ϕ_1	ϕ_2	ϕ_1	at most 1
Type Z	ϕ_1	ϕ_2	ϕ_3	none

Table 1: The different NFC-respecting Yukawa structures for the $\mathbb{Z}_2 \times \mathbb{Z}_2$ -symmetric 3HDM.

In democratic models, all three vevs must be non-zero in order for fermions to be massive whereas in other types one or two doublets may have a vanishing vev and thus lead to dark-matter candidates [17–19].

Consider the generic Yukawa Lagrangian (the indices a , b and c do not need to be different)

$$-\mathcal{L}_Y = \bar{Q}_L^0 Y^u \tilde{\phi}_a u_R^0 + \bar{Q}_L^0 Y^d \phi_b d_R^0 + \bar{E}_L^0 Y^e \phi_c e_R^0 + \text{h.c.}, \quad (5.1)$$

where the superscript “0” on fermion fields is a reminder that these are not necessarily mass eigenfields. Even though the vevs may be complex, the complex phases may be absorbed by a redefinition of the right-handed fermion fields and hence play no role in the Yukawa interactions. This is a generic feature of models with NFC.

In addition to providing the fermion mass matrices

$$\frac{v_a}{\sqrt{2}} Y^f = m_f, \quad (5.2)$$

this Lagrangian will determine the interactions between the fermions and the physical scalar fields of Eq. (2.4). Below, we write these interactions in the fermion physical basis where $m_f = \text{diag}(m_{f_1}, m_{f_2}, m_{f_3})$, with $f \in \{u, d, e\}$.

We will parametrize the interaction of fermions with neutral scalars as

$$-\mathcal{L}_Y \supset \bar{f} \frac{m_f}{v} (\kappa_{h_i f f}^S \pm i \kappa_{h_i f f}^P \gamma_5) f h_i \quad i = 1, \dots, 5, \quad (5.3)$$

with

$$\kappa_{h_i f f}^S = \frac{v}{v_a} \mathcal{O}_{ia}, \quad \kappa_{h_i f f}^P = \frac{v}{v_a} \mathcal{O}_{i a+3}. \quad (5.4)$$

The “ \pm ” sign in Eq. (5.3) should be interpreted as “plus” for d -type quarks (and charged leptons) and “minus” for u -type quarks, and stems from the complex conjugation associated with the $\tilde{\phi}$ factor in Eq. (5.1). Furthermore, \mathcal{O} is the diagonalization matrix, defined in Eq. (2.4).

For the purpose of studying the $b \rightarrow s\gamma$ constraint, it is convenient to write the interaction of the quarks with the charged scalars in the notation of Borzumati and Greub [20],

$$-\mathcal{L}_Y \supset \frac{g}{\sqrt{2} m_W} \sum_{i,j,k} V_{ij} \left\{ \bar{u}_i [Y_k m_{u_i} P_L + X_k m_{d_j} P_R] d_j h_k^+ + \text{h.c.} \right\}. \quad (5.5)$$

The notation of Ciuchini, Degrandi, Gambino and Giudice [21, 22] is also often used:

$$-\mathcal{L}_Y \supset (2\sqrt{2} G_F)^{1/2} \sum_{i,j,k} V_{ij} \left\{ \bar{u}_i [A_u^k m_{u_i} P_L - A_d^k m_{d_j} P_R] d_j h_k^+ + \text{h.c.} \right\}. \quad (5.6)$$

Here,

$$\frac{g}{\sqrt{2} m_W} = \frac{\sqrt{2}}{v} = (2\sqrt{2} G_F)^{1/2}, \quad (5.7)$$

G_F is the Fermi constant, and V_{ij} the appropriate element of the CKM matrix. The coefficients X_k and Y_k do not depend either on quark mass or on the CKM matrix element. However, they will depend on which type of Yukawa couplings we consider, as specified in the following. The subscript k refers to the charged scalar, $k = 1, 2$.

The two notations (5.5) and (5.6) are related by

$$X_k = -A_d^k, \quad Y_k = A_u^k. \quad (5.8)$$

5.1 Type I Yukawa couplings

With both u - and d -quarks (as well as charged leptons) coupling to ϕ_a , we find

$$Y_k = \frac{v}{v_a} \mathcal{U}_{ka}^*, \quad X_k = -\frac{v}{v_a} \mathcal{U}_{ka}, \quad \text{no sum over } a. \quad (5.9)$$

For comparison, in the familiar 2HDM with Type I Yukawa couplings we have

$$Y = \frac{1}{\tan \beta}, \quad X = -Y. \quad (5.10)$$

The 2HDM values are obtained if we consider $v_a \rightarrow v_2 = v \sin \beta$, and $\mathcal{U}_{ka} \rightarrow \cos \beta$, with β the rotation angle identifying the Goldstone boson in the 2HDM.

5.2 Type II Yukawa couplings

With u - and d -quarks (as well as charged leptons) coupling to ϕ_a and ϕ_b , respectively, we find

$$Y_k = \frac{v}{v_a} \mathcal{U}_{ka}^*, \quad X_k = \frac{v}{v_b} \mathcal{U}_{kb}, \quad \text{no sum over } a, \text{ with } b \neq a. \quad (5.11)$$

For fixed v_a and v_b , $|Y_k|$ and $|X_k|$ will be proportional. In the familiar 2HDM we have

$$Y = \frac{1}{X} = \frac{1}{\tan \beta}. \quad (5.12)$$

5.3 Type Z Yukawa couplings

With u - and d -quarks coupling to ϕ_a and ϕ_b , respectively, and charged leptons coupling to ϕ_c , we find Y_k and X_k like for Type II, and for charged leptons

$$Z_k = \frac{v}{v_c} \mathcal{U}_{kc}, \quad \text{no sum over } c \neq a, b. \quad (5.13)$$

We show, in Fig. 1, scatter plots of the measures of CP violation, A_{sum} (grey, bottom layer, mostly covered), A_{max} (blue, over grey), defined by Eq. (4.7), vs θ_2/π and θ_3/π , based on the scan performed in Ref. [2]. The cut-off at high values is obviously caused by the upper bounds on the λ s (from perturbativity). Likewise, there is a thinning out at low values due to the finite resolution in the scan sample. Inspection shows that the lower points are associated with low masses of the lightest neutral state. This is reminiscent of the 2HDM case [14] where the corresponding invariants are proportional to masses squared or even differences of masses squared.

Actually, the original scan [2] does not have any lower bound imposed on the masses of the neutral scalars. In order to explore this connection, we imposed a lower bound of 45 GeV on the lightest neutral scalar, and obtained the subset of points shown in yellow (on top of the blue). It appears that in order to have “little” CP violation (points in the lower part of the plot), some neutral scalars must be light.

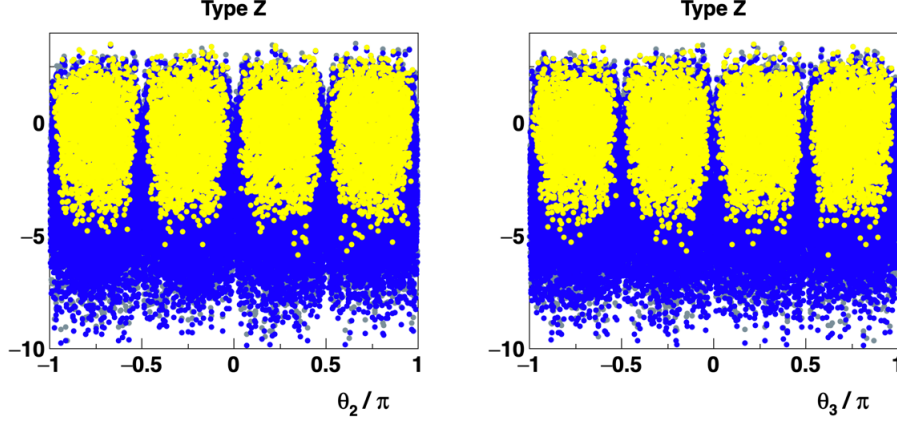


Figure 1: Scatter plots of logarithms of the sum (and maxima) of the squares of the 15 invariants of Eq. (4.3) vs θ_2 and θ_3 . See the text for comments.

6 Experimental constraints

We shall here impose further experimental constraints on the parameter points which already survived the following constraints [2]: compatibility with the measured $WW h_{\text{SM}}$ coupling [23] and the CP constraint on the $h_{\text{SM}} \rightarrow \bar{\tau}\tau$ coupling [24]. Now, we also impose the constraints from the electroweak precision observables, S , T and U , from the digamma signal strength ($h_{\text{SM}} \rightarrow \gamma\gamma$), from $\bar{B} \rightarrow X_s \gamma$ and from the electron EDM.

6.1 Electroweak precision observables

The oblique parameters S, T, U parametrize possible BSM deviations in the electroweak precision observables [25–27] and have been calculated for a general multi-Higgs model consisting of SU(2) doublets and singlets [28, 29]. We take into account the correlation between S and T , and adopt the 2-sigma contours from [30] which are based on a χ^2 fit of the electroweak precision observables with respect to their PDG values [23].

6.2 $h_i \rightarrow \gamma\gamma$

For the SM Higgs particle, the one-loop diphoton decay width has long been known [31–33] and played an important role in its discovery. The $h_i WW$ vertex coupling will slightly differ from the SM value. Furthermore, there will be an additional contribution to $h_i \rightarrow \gamma\gamma$ coming from one-loop processes involving the charged scalars. This new contribution will interfere with the one-loop SM processes involving fermions and the W boson and could enhance or reduce the total decay rate.

For the Weinberg potential the relevant part of the Lagrangian for this process is [2]

$$\mathcal{L}_{h_i\gamma\gamma} = gm_W O_{i1} h_i W_\mu^+ W^{\mu-} - \frac{m_f}{v} (\kappa_{h_i f f}^S h_i \bar{f} f + i\kappa_{h_i d d}^P h_i \bar{d} \gamma_5 d - i\kappa_{h_i u u}^P h_i \bar{u} \gamma_5 u)$$

$$- \sum_{k,k'=1,2} v g_{ikk'} h_i h_k^+ h_{k'}^- . \quad (6.1)$$

Here, and in Eq. (6.3) below, O_{i1} is an element of the rotation matrix, given by Eq. (A.5) in appendix A. Since the neutral scalars are mixed CP states, their scalar and pseudoscalar Yukawa couplings $\kappa_{h_i f f}^{S,P}$ are in general both non-zero. Reading off the coupling modifiers, the decay rate is given by [33, 34]

$$\Gamma(h_i \rightarrow \gamma\gamma) = \frac{\alpha^2}{256\pi^3} \frac{m_i^3}{v^2} \{ |I_1 + I_{1/2}^S + I_0|^2 + |I_{1/2}^P|^2 \}, \quad (6.2)$$

where the W -loop contribution is given by

$$I_1 = O_{i1} F_1(\tau_W), \quad (6.3)$$

the fermion loop contributions are given by²

$$I_{\frac{1}{2}}^r = \sum_f N_c^f e_f^2 \kappa_{h_i f f}^r F_{\frac{1}{2}}^r(\tau_f), \quad r = S, P, \quad (6.4)$$

and the contributions of the charged scalars by

$$I_0 = \sum_{k=1,2} \frac{v^2}{2m_{h_k^\pm}^2} g_{ikk} F_0(\tau_{h_k^\pm}). \quad (6.5)$$

Here, N_c^f and e_f refer to the color multiplicity and electric charge of fermion f , respectively, $\tau_j = 4m_j^2/m_i^2$ and the functions F are the one-loop functions given in [33]. We adopt values for $\mu_{\gamma\gamma} = \Gamma(h_i \rightarrow \gamma\gamma)/\Gamma(h_{\text{SM}} \rightarrow \gamma\gamma)$ within 3σ of the PDG result $\mu_{\gamma\gamma} = 1.10 \pm 0.07$ [23] for the h_i that is interpreted as h_{SM} (h_2 or h_3).

6.3 $\bar{B} \rightarrow X_s \gamma$

The importance of charged scalar exchange for the $\bar{B} \rightarrow X_s \gamma$ rate has been known since the late 1980's [35–37]. The rate is determined from an expansion of the relevant Wilson coefficients in powers of $\tilde{\alpha}_s \equiv \alpha_s/(4\pi)$, starting with (1) the matching of these coefficients to the full theory at a high scale ($\mu_0 \sim m_W$ or m_t), then (2) evolve them down to the low scale $\mu_b \sim m_b$ (taking into account the mixing of operators in this process), and (3) determine the matrix elements at the low scale [20–22, 38–48].

The Weinberg potential, with the general vacuum we are considering, has *two* pairs of charged scalars. This means that there are two charged-scalar contributions to the $\bar{B} \rightarrow X_s \gamma$ decay amplitude. For the 2HDM, with just one charged scalar³, the calculation of this branching ratio is already rather complicated, involving a BSM contribution to the

²There is a sign ambiguity associated with this contribution. We allow for either sign. For a given parameter set, only one sign admits agreement with observations, usually the SM sign.

³Or 3HDM's with only one active charged scalar.

amplitude that contains a $bH^{\pm}t$ and an $sH^{\pm}t$ (or a $bH^{\pm}c$ and an $sH^{\pm}c$) coupling, subject to large QCD corrections [22], plus a non-perturbative part.

Since the experimental data are in good agreement with the most precise SM calculations, the BSM contribution has to be small. This imposes constraints on the above-mentioned couplings (in the 2HDM, these are often expressed in terms of $\tan\beta$) and the charged-Higgs mass (a high mass will suppress this loop contribution).

The minimisation conditions of the potential, Eq. (3.12), force all mass terms in the potential to be fully written in terms of the quartic couplings [2], and since the latter are constrained by perturbativity, the masses of the charged scalars are at the order of the electroweak scale. This will have an impact on the $\bar{B} \rightarrow X_s \gamma$ constraint.

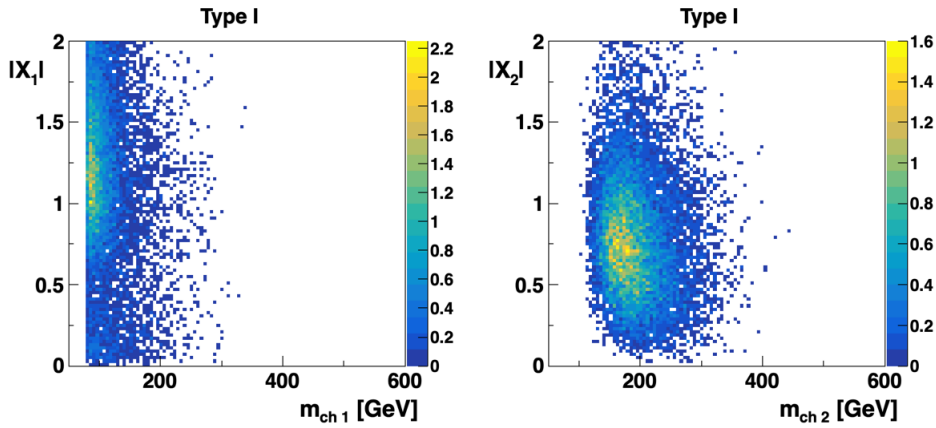


Figure 2: Scatter plots of the moduli $|X_k| = |Y_k|$ (see Eq. (5.5)) vs the charged-scalar masses for Type I Yukawa couplings.

6.3.1 The $b\bar{t}h_k^+$ couplings

As a first step in acquiring some intuition for this constraint based on the considered potential, we show in Fig. 2 scatter plots of the Type I couplings $|X_k| = |Y_k|$, defined by Eq. (5.5), vs the charged-scalar mass. The points shown satisfy the theoretical constraints, as well as the electroweak S , T , U constraints, and the digamma rate.

A new feature (as compared with the familiar 2HDMs) is that there are *two* charged states. There could thus be regions of parameter space in which the contributions of the two charged scalars h_1^+ and h_2^+ have opposite signs, and partially cancel, allowing for rather light charged-scalar masses without violating the $\bar{B} \rightarrow X_s \gamma$ constraint [49].

6.3.2 Treatment of the $\bar{B} \rightarrow X_s \gamma$ constraint

As mentioned above, compared to the familiar $\bar{B} \rightarrow X_s \gamma$ constraint for the 2HDM, we here face two complications:

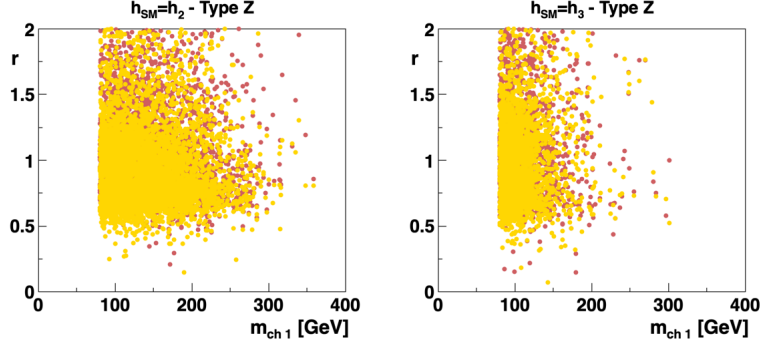


Figure 3: Scatter plots of relative sums r defined as the ratio between the absolute value of (6.7) and the absolute value of the first term ($k = 1$). Reddish: ratios r for C_7 , yellowish (on top): for C_8 . Left: $h_2 = h_{\text{SM}}$, right: $h_3 = h_{\text{SM}}$. See the text for more comments.

- The couplings X_k and Y_k are complex. Thus, some Wilson coefficients will become complex.
- There are two charged scalars, thus two non-SM contributions to the *amplitude* determining the decay rate.

The basic BSM contribution to the amplitude for $\bar{B} \rightarrow X_s \gamma$ involves the couplings X and Y in the following combination for both Wilson coefficients C_7 and C_8 [20],

$$f(y)|Y|^2 + g(y)(X^*Y), \quad (6.6)$$

where for the lowest-order (in $\tilde{\alpha}_s$) amplitude $f(y)$ and $g(y)$ are just Inami-Lim functions [50] of the ratio $y = (m_t/m_{h^\pm})^2$, whereas at the NLO level they are more complicated functions. Loop contributions involving both charged scalars will obviously interfere at the amplitude level. Thus, in order to account for both charged scalars, we replace the expression (6.6) (at the high scale, often referred to as μ_0) by

$$\sum_{k=1}^2 [f(y_k)|Y_k|^2 + g(y_k)(X_k^*Y_k)], \quad (6.7)$$

both at the LO and the NLO level.

In order to explore the possible cancellations, in Fig. 3 we show the ratios

$$r = \frac{|\sum_{k=1}^2 [f(y_k)|Y_k|^2 + g(y_k)(X_k^*Y_k)]|}{|f(y_1)|Y_1|^2 + g(y_1)(X_1^*Y_1)|} \quad (6.8)$$

for contributions to C_7 and to C_8 , for both $h_2 = h_{\text{SM}}$ and $h_3 = h_{\text{SM}}$. Only parameter points surviving the previous constraints including $\bar{B} \rightarrow X_s \gamma$ are shown. A considerable fraction of the surviving scan points lie below unity, i.e., representing cases of destructive interference between the contributions of h_1^\pm and h_2^\pm .

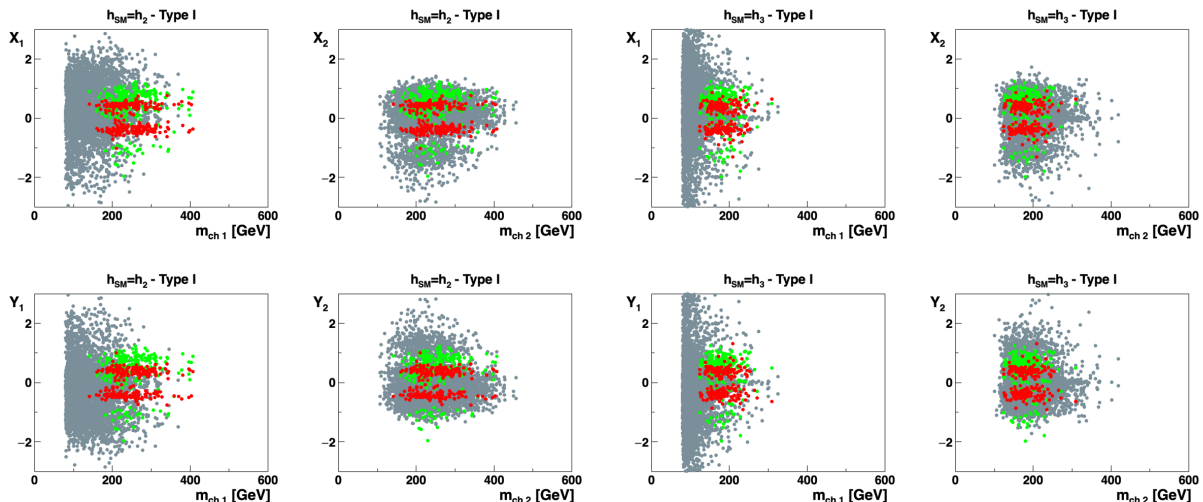


Figure 4: Scatter plots of real (green) and imaginary (red, on top of green) parts of X_k and Y_k vs the charged-scalar masses for Type I Yukawa couplings, with h_2 (left) or h_3 (right) identified as h_{SM} . See text for more details.

Next, we show in Figs. 4 and 5 scatter plots of real and imaginary parts of X_k and Y_k vs $m_{\text{ch } k}$, for Type I and Type Z Yukawa couplings. In grey, as an underlying background, we show real and imaginary parts of these couplings for parameter points that survive all previous constraints, not considering $\bar{B} \rightarrow X_s \gamma$. Superimposed on this background, we show separately real (green) and imaginary (red) parts of X_k and Y_k that in addition survive an approximate implementation of the $\bar{B} \rightarrow X_s \gamma$ constraint $\text{Br}(\bar{B} \rightarrow X_s \gamma) \times 10^4 = 3.32 \pm 0.15$ [23] at the $3\text{-}\sigma$ level. The points are layered in the following sequence. Bottom, grey: no $\bar{B} \rightarrow X_s \gamma$ constraints; intermediate, green: real part; top, red: imaginary part. Grey points come in pairs. For each green point there is also a red point.

The cases $h_2 = h_{\text{SM}}$ (left, $k = 1$ and 2) and $h_3 = h_{\text{SM}}$ (right, $k = 1$ and 2) are considered. Figure 5, labelled “Type Z”, applies equally to Type II Yukawa couplings since the Yukawa couplings to leptons have no bearing on the $\bar{B} \rightarrow X_s \gamma$ constraint. In evaluating the constraints, we include interference with the SM amplitude, up to the second order in $\tilde{\alpha}_S$ [51].

The red bands in Fig. 4 (Type I) show that non-zero imaginary parts of X_k and Y_k are required for the $\bar{B} \rightarrow X_s \gamma$ constraint to be satisfied. This is no longer the case in Fig. 5 (Type Z). For Type I Yukawa couplings we observe both lower and upper bounds on $|\text{Im } X_k|$ and $|\text{Im } Y_k|$, whereas for Type Z we observe only upper bounds.

6.4 The electron EDM

The mixing of CP-even and odd fields will induce a contribution to the electron electric dipole moment via the Barr–Zee effect [52], which is experimentally rather constrained. Following Pilaftsis [53], the result can be expressed in terms of the couplings κ^S and κ^P of

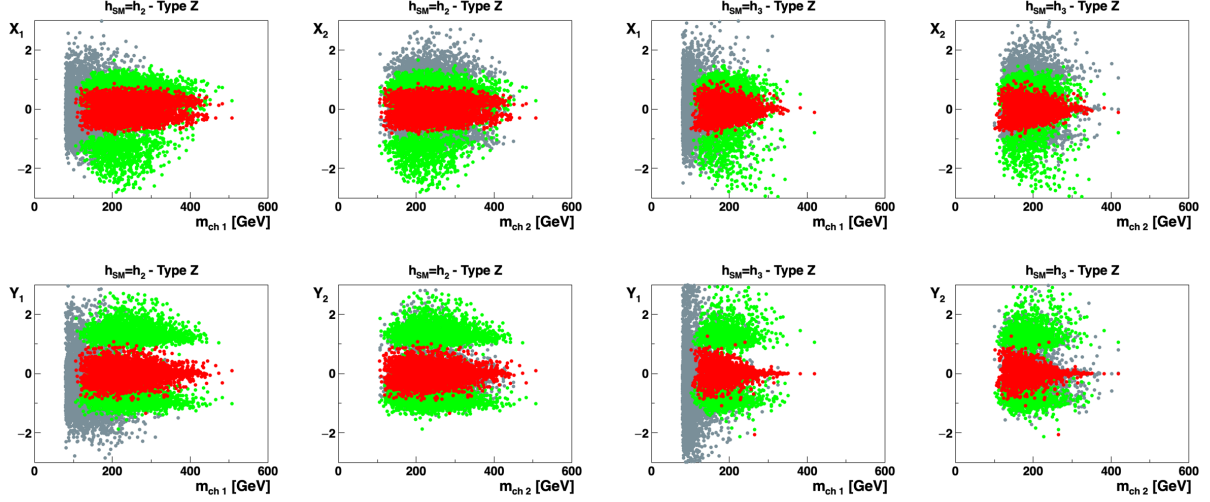


Figure 5: Scatter plots of real (green) and imaginary (red, on top of green) parts of X_k and Y_k vs the charged-scalar masses for Type Z (or Type II) Yukawa couplings, with h_2 (left) or h_3 (right) identified as h_{SM} . See text for more details.

Eq. (6.1) as

$$\frac{d_e}{e} = -\frac{3\alpha_{\text{e.m.}}}{8\pi^2 \sin^2 \theta_W} \frac{m_e}{m_W^2} \sum_{i=1}^5 \sum_{q=t,b} Q_q^2 \left[\kappa_{h_i e e}^P \kappa_{h_i q q}^S f\left(\frac{m_q^2}{m_{h_i}^2}\right) + \kappa_{h_i e e}^S \kappa_{h_i q q}^P g\left(\frac{m_q^2}{m_{h_i}^2}\right) \right]. \quad (6.9)$$

Here, f and g are two-loop functions [52], not to be confused with the f and g of Eqs. (6.6)–(6.8). The experimental upper bound has recently been tightened from $1.1 \times 10^{-29} e \cdot \text{cm}$ [54] to $4.1 \times 10^{-30} e \cdot \text{cm}$ [55].

The SM contribution to this process, induced by a complex CKM matrix is of the order $10^{-38} e \cdot \text{cm}$ which is much smaller than the scalar contribution of the present model. Therefore we do not consider at this stage what mechanism would generate a complex CKM matrix.

Since the complex vevs induce a mixing of the CP even and odd fields, it is interesting to see how $|d_e/e|$ varies with the phases of the vevs. We show in Fig. 6 parameter points for which $|d_e/e| < 10^{-27} e \cdot \text{cm}$ vs θ_2 and θ_3 . While the distribution is thinning out at low values of $|d_e|$, there are parameter points for which $|d_e/e| < 10^{-29} e \cdot \text{cm}$, as required by experiment.

Since a non-zero d_e is a sign of CP violation, and CP is conserved in the limits $\theta_i = n\pi/2$, one would expect parameter points of small $|d_2|$ to be found near these limits. This is however not the case, due to other constraints, as discussed in section 9.2.

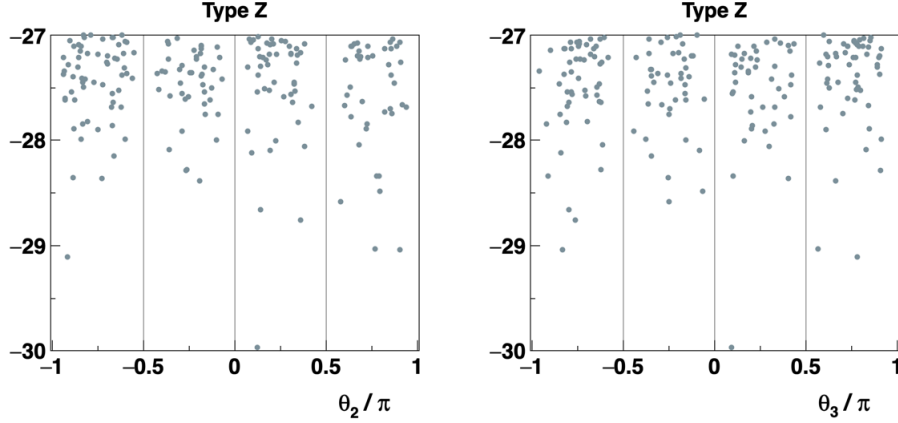


Figure 6: Scatter plots of logarithms of the electron EDM vs the angles θ_2 and θ_3 .

7 CP violation—the invariants

The experimental upper bound on the electric dipole moment is an important constraint on CP-violating theories. We shall here explore how this constraint is reflected in the CP-violating invariants presented in section 4. The Yukawa couplings $\kappa_{h_{i}ff}^P$ which would vanish for real vevs, are clearly related to the invariants. While we there (in section 4) presented a global measure, involving all 15 invariants of Eq. (4.3), we shall here explore the individual invariants, and see how they correlate with the value of the electric dipole moment.

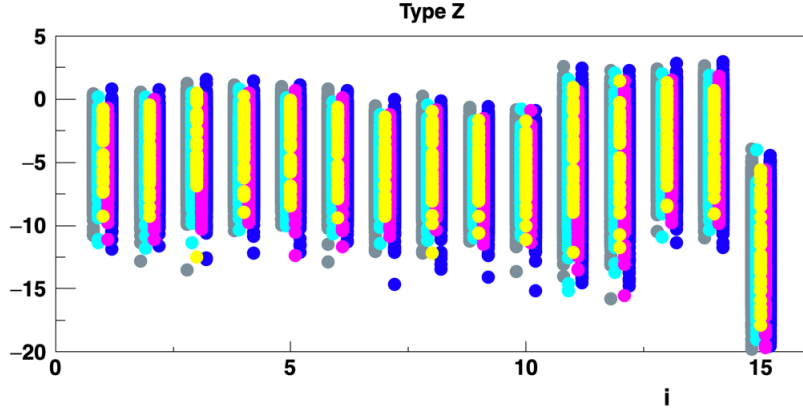


Figure 7: Scatter plots of $\log_{10}(J_i^2)$ for the 15 invariants of Eq. (4.3). Different colours denote different ranges of $|d_e|$ as specified by the list (7.1).

In Fig. 7 we show scatter plots of $\log_{10}(J_i^2)$ vs i , for i ranging from 1 to 15, where the points are colour coded according to the range of the electric dipole moment d_e as follows

(a small horizontal offset is introduced to improve readability):

grey (bottom layer)	$ d_e /e < 10^{-27}$ cm, and $(\tan \alpha)_\tau < 0.1$ [2],	
blue	$ d_e /e < 5 \cdot 10^{-28}$ cm,	
green	$ d_e /e < 10^{-28}$ cm,	(7.1)
purple	$ d_e /e < 5 \cdot 10^{-29}$ cm,	
yellow (on top)	$ d_e /e < 10^{-29}$ cm.	

The invariant J_{15} , which involves the bilinear terms in the potential, is overall smaller than the others. While these scatter plots reflect their underlying stochastic nature from the finite number of scan points, there is an interesting correlation of the *maximum* values with the range of $|d_e|$. In fact, as $|d_e|$ is constrained to successively smaller values, *all* J_i invariant are also constrained in the sense that the maximum is lower.

We see that a constraint on *one* CP-violating observable (here: $|d_e|$) impacts *all* the CP-violating invariants. In order to illustrate this connection, we split the range of d_e values into bins, analogous to those of Eq. (7.1), and plot for each of the 15 J_i the maximum value of $\log_{10}(J_i^2)$ in each bin of d_e -values, using a different colour code. The result is shown in Fig. 8.

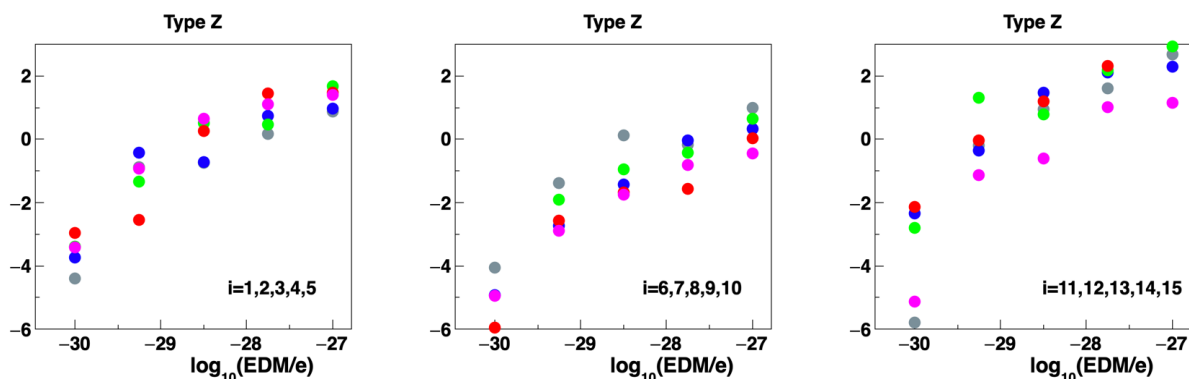


Figure 8: Plots of $\max(\log_{10}(J_i^2))$ for the 15 invariants of Eq. (4.3). The maximum value of the invariant within each EDM bin is plotted. Different colours refer to different J_i . Each frame displays the result for invariants appearing in increasing order of i . Grey: $i = 1, 6, 11$; blue: $i = 2, 7, 12$; green: $i = 3, 8, 13$; red: $i = 4, 9, 14$; purple: $i = 5, 10, 15$. For $i = 15$, we have shifted the values upwards by 5 units (see Fig. 7).

Apart from some fluctuations due to the finite scan sample, there is a clear tendency for the maximum value of the invariants to get smaller in bins of smaller values of $|d_e|$. And, importantly, we see that the potential is able to produce models with d_e below $10^{-29}e \cdot \text{cm}$ as required by recent data.

What this shows is that the simple basis of invariants chosen in Eq. (4.3) is not well “aligned” with this particular observable, an invariant describing only the EDM would be a linear combination of those given in Eq. (4.3).

8 Two CP-violating processes

We shall next comment on two CP non-conserving processes,

$$W^+W^- \rightarrow Z, \quad (8.1)$$

$$h_i^+ h_i^- \rightarrow h_1^\pm h_2^\mp, \quad (8.2)$$

the first of which could perhaps be experimentally accessible, whereas the second one is more of academic interest. However, it has the unique feature of involving only scalar particles in the initial and final states, no fermions and no gauge bosons.

8.1 $W^+W^- \rightarrow Z$

For the WWZ vertex we adopt the notation given in Fig. 9, with all momenta incoming.

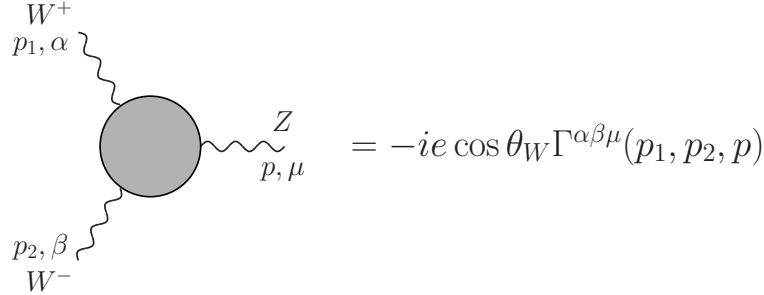


Figure 9: The general WWZ vertex.

The vertex is present at the tree level, with a well-known, CP-conserving structure:

$$\begin{aligned} ig_{WWZ}\Gamma_{\text{tree}}^{\mu_1\mu_2\mu} &= -ig \cos \theta_W [g^{\mu_1\mu_2}(p_2 - p_1)^\mu + g^{\mu_2\mu}(p - p_2)^{\mu_1} + g^{\mu\mu_1}(p_1 - p)^{\mu_2}] \\ &= -ig \cos \theta_W [g^{\mu_1\mu_2}\ell^\mu + g^{\mu_2\mu}(\tfrac{3}{2}p - \tfrac{1}{2}\ell)^{\mu_1} - g^{\mu\mu_1}(\tfrac{3}{2}p + \tfrac{1}{2}\ell)^{\mu_2}], \end{aligned} \quad (8.3)$$

where $g_{WWZ} = -e \cot \theta_W$, and in the second line, we make use of the abbreviation $\ell = p_2 - p_1$.

Triangle diagrams discussed below contribute to CP-violation in the W^+W^-Z vertex. In fact, in the Two-Higgs-Doublet model they give a contribution proportional to the 2HDM-invariant $\text{Im } J_2$, which is one measure of CP violation [10, 11] (referred to as J_1 in earlier work by Lavoura, Silva and Botella [8, 9]), not to be confused with the J_i of Eq. (4.3).

Phenomenological discussions [56] of the WWZ vertex have presented its most general Lorentz structure. We assume both W^\pm to be on-shell and Z off-shell, furthermore assuming that Z couples to a pair of light leptons like e^+e^- so that we may neglect terms proportional to the lepton mass. Then, according to [56] the structure reads

$$\Gamma_{WWZ}^{\alpha\beta\mu} = f_1^Z \ell^\mu g^{\alpha\beta} - \frac{f_2^Z}{m_W^2} \ell^\mu p^\alpha p^\beta + f_3^Z (p^\alpha g^{\mu\beta} - p^\beta g^{\mu\alpha})$$

$$\begin{aligned}
& + i f_4^Z (p^\alpha g^{\mu\beta} + p^\beta g^{\mu\alpha}) + i f_5^Z \epsilon^{\mu\alpha\beta\rho} \ell_\rho \\
& - f_6^Z \epsilon^{\mu\alpha\beta\rho} p_\rho - \frac{f_7^Z}{m_W^2} \ell^\mu \epsilon^{\alpha\beta\rho\sigma} p_\rho \ell_\sigma.
\end{aligned} \tag{8.4}$$

The tree-level vertex contributes to f_1 and f_3 :

$$f_1^{\text{tree}} = 1, \quad f_3^{\text{tree}} = 2. \tag{8.5}$$

The dimensionless form factors f_4^Z , f_6^Z and f_7^Z violate CP while the others conserve CP [56]. LHC experiments [57, 58] have constrained the CP-conserving anomalous couplings f_2^Z and f_5^Z , and even started to constrain the CP-violating f_4^Z to below 0.0015 [59].

In the CP-violating 2HDM there are contributions to f_4^Z that arise from triangle diagrams of the kind shown in Fig. 10 [60]. Like for the ZZZ vertex, this contribution is proportional to the product of the three VVh couplings, $e_1 e_2 e_3$ (see Table 2 and ref. [14]), and it was shown that it is also proportional to the differences of masses squared that make up the invariant $\text{Im } J_2$, resulting in $f_4^Z \propto \text{Im } J_2$.

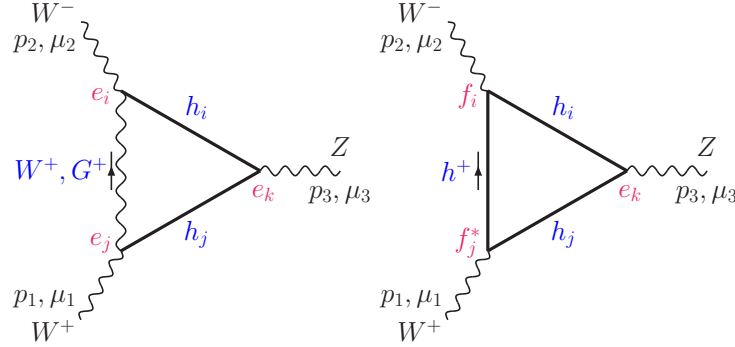


Figure 10: Loop contributions to the CP-violating $W^+W^- \rightarrow Z$ amplitude in the 2HDM

In the framework of the 3HDM, and in particular in the case of the Weinberg potential, the situation is more complicated for several reasons. Diagrams corresponding to the one given in Fig. 10 for the 2HDM are shown in Fig. 11 for a 3HDM.

	2HDM	3HDM
$Zh_i h_j$	$\epsilon_{ijk} e_k$	λ_{ij}
ZZh_k	e_k	e_k

Table 2: Trilinear vector-scalar couplings (the $Zh_i h_j$ coupling was referred to as P_{ij} in [2, 3]), modulo normalization and Lorentz structure.

In the 2HDM, the relevant part of the product $f_i f_j^*$ can be expressed in terms of $e_i e_j$ and the $Zh_i h_j$ couplings⁴ λ_{ij} can be expressed in terms of $\epsilon_{ijk} e_k$, i.e., the VVh_k -couplings. This is not the case in a 3HDM. In a 3HDM, we have five couplings e_i and

⁴Here, and in Fig. 11 and Table 2, the two-index λ refers to the coupling of a vector boson with two neutral scalars. It should not be confused with any λ appearing in the potential.

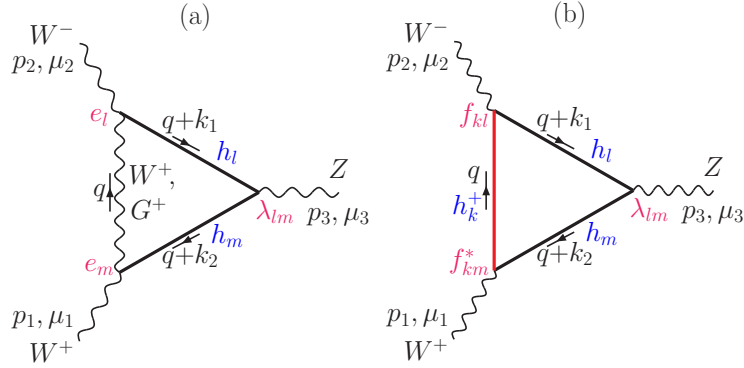


Figure 11: Loop contributions to the CP-violating $W^+W^- \rightarrow Z$ amplitude

ten couplings λ_{ij} . However, there exist relations between the e_i and the λ_{ij} that can be used to show that the number of independent couplings are not $5+10=15$, but in fact the number of independent neutral gauge couplings is only 7. One can for instance pick the seven independent couplings to consist of the five e_i along with two of the λ_{ij} . Then, the remaining eight λ_{ij} can always be expressed in terms of the seven independent couplings that we pick. Since these relations between the different gauge couplings are not as transparent in a 3HDM as in a 2HDM, we will just express the results in terms of the five e_i and the ten λ_{ij} . See appendix D.

In the 2HDM, the CP-odd contribution to the ZWW vertex was directly proportional to the CP-odd invariant $\text{Im } J_2$ (expressed in terms of masses and gauge couplings). In the 3HDM, one can also express the CP-odd contribution to the ZWW -vertex in terms of similar CP-odd invariants translated into a sum involving a combination of masses and the couplings appearing in the triangle diagrams. We did not calculate the contribution to the CP-odd form factor for our model, but we expect it to be a linear combination of CP-odd invariants J_i , where we include not only the 15 invariants of the theorem, but also those extra ones that are needed in order to form a “linear algebraic basis” for all the CP-odd invariants of the model (see Section 4). CP-odd invariants that appear in those contributions are not necessarily the same as the set of invariants J_1, \dots, J_{15} whose simultaneous vanishing implies CP-conservation, but they will all vanish simultaneously with J_1, \dots, J_{15} .

8.2 A Gedanken Experiment: $h_i^+ h_i^- \rightarrow h_1^\pm h_2^\mp$

Typically, CP violation involves fermions. In the 2HDM, CP violation can take place in the non-fermionic sector, and will often involve the couplings to gauge bosons [7, 8] (see also [14]). In a recent study [61], it was pointed out that the simultaneous observation of three non-vanishing processes constitutes evidence for P-even CP-violating scalar exchange. But in that study, couplings to gauge bosons are essential. We shall here present a charge asymmetry that would constitute a P-even CP violation, not involving gauge bosons.

The Weinberg potential allows for CP violation in the scalar sector, without involvement

of either fermions or gauge bosons. We believe this phenomenon is novel, and will present a schematic description in the following. The CP violation induced on the scalar sector by the complex vevs can be explored by comparing the two processes

$$h_i^+ h_i^- \rightarrow h_1^+ h_2^-, \quad \text{and} \quad (8.6a)$$

$$h_i^+ h_i^- \rightarrow h_1^- h_2^+. \quad (8.6b)$$

Importantly, the initial state is even under CP, whereas the final state is not an eigenstate of CP since h_1^\pm and h_2^\pm have different masses. While it may be hard to imagine actually measuring this asymmetry, it is interesting to see how the different couplings can conspire to produce a non-zero result.

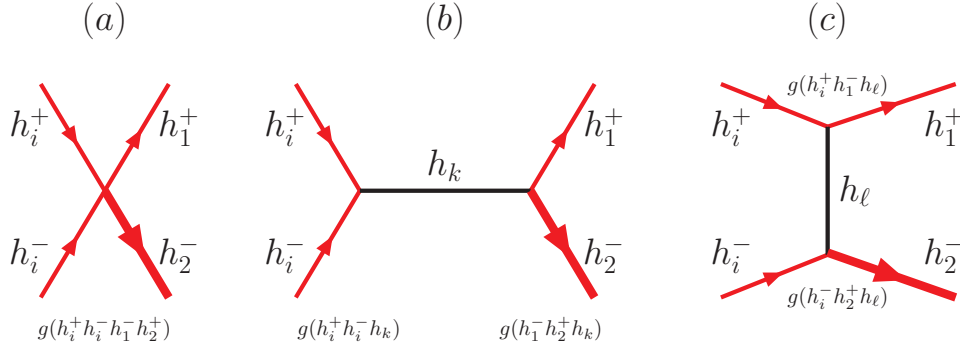


Figure 12: Feynman diagrams contributing to $h_i^+ h_i^- \rightarrow h_1^+ h_2^-$. The couplings g refer to the related process where all fields are incoming.

At tree level, the process may proceed via the diagrams shown in Fig. 12 with the amplitudes

$$\mathcal{M}_{\text{tree}}(h_i^+ h_i^- \rightarrow h_1^+ h_2^-) = -ig(h_i^+ h_i^- h_1^+ h_2^-) + \mathcal{M}_b^{+-} + \mathcal{M}_c^{+-}, \quad (8.7a)$$

$$\mathcal{M}_{\text{tree}}(h_i^+ h_i^- \rightarrow h_1^- h_2^+) = -ig(h_i^+ h_i^- h_1^- h_2^+) + \mathcal{M}_b^{-+} + \mathcal{M}_c^{-+}, \quad (8.7b)$$

where $i = 1$ or 2 refers to the initial state and the subscripts “b” and “c” refer to the diagrams in Fig. 12. Furthermore,

$$\mathcal{M}_b^{+-} = \sum_{k=1}^5 [-ig(h_i^+ h_i^- h_k)] \frac{i}{s - m_k^2} [-ig(h_2^+ h_1^- h_k)], \quad (8.8a)$$

$$\mathcal{M}_c^{+-} = \sum_{\ell=1}^5 [-ig(h_i^+ h_1^+ h_\ell)] \frac{i}{t - m_\ell^2} [-ig(h_2^+ h_i^- h_\ell)], \quad (8.8b)$$

where $g(xyz)$ refers to the trilinear coupling of fields x , y and z . While the Feynman diagrams are drawn in terms of outgoing particles in the final state, we define the vertices $g(xyz)$ in terms of all fields being incoming.

Replacing fields by their charge conjugated ones, individual vertex couplings will be replaced by their complex conjugated ones,

$$g(h_i^+ h_i^- h_1^+ h_2^-) = [g(h_i^+ h_i^- h_1^- h_2^+)]^* \quad \text{and} \quad g(h_2^+ h_1^- h_k) = [g(h_2^- h_1^+ h_k)]^*. \quad (8.9)$$

Charge-symmetric vertices are real. In a CP-conserving theory, in diagram (b), only a CP-even h_k would couple to the initial state, and thus only couple to the CP-even part of $h_1^\pm h_2^\mp$. Here, however, since h_k has indefinite CP, it can couple to both the CP-even and the CP-odd part of the final state. The same is obviously true for the h_ℓ in the t -channel.

Thus, the two expressions in (8.7) are related by complex conjugation as follows (the kinematical variable t will not change):

$$i\mathcal{M}_{\text{tree}}(h_i^+ h_i^- \rightarrow h_1^- h_2^+) = [i\mathcal{M}_{\text{tree}}(h_i^+ h_i^- \rightarrow h_1^+ h_2^-)]^*, \quad (8.10)$$

and the two rates (8.6) will be the same at tree level.

In fact, the amplitudes can be expanded as follows,

$$\mathcal{M}(h_i^+ h_i^- \rightarrow h_1^+ h_2^-) = -i \sum_k A_k g_k(h_1^+ h_2^-), \quad (8.11a)$$

$$\mathcal{M}(h_i^+ h_i^- \rightarrow h_1^- h_2^+) = -i \sum_k A_k g_k(h_1^- h_2^+), \quad (8.11b)$$

where

$$g_k(h_1^- h_2^+) = g_k(h_1^+ h_2^-)^* \quad \text{for all } k. \quad (8.12)$$

At tree level the A_k are all real, composed of real charge-symmetric couplings and propagators, leading to Eq. (8.10) and the equality of the two rates.

However, at loop level, some A_k will involve a loop integral, and thus in general be complex, given by the *same* complex function for both charge configurations. Thus, the two amplitudes $\mathcal{M}(h_i^+ h_i^- \rightarrow h_1^+ h_2^-)$ and $\mathcal{M}(h_i^+ h_i^- \rightarrow h_1^- h_2^+)$ of Eq. (8.11) will *not* be related by complex conjugation, the two rates of Eq. (??) will differ.

It should be noted that this CP asymmetry originates in the scalar sector, as a C asymmetry. No parity violating observable can be constructed involving only scalars. In reality, however, also other exchanges would contribute to the asymmetry, such as gauge bosons and fermions.

For the CP-odd contribution to the ZWW vertex, we argued that the amplitude itself would contain linear combinations of CP-odd invariants J_i . For the $h_i^+ h_i^- \rightarrow h_1^\pm h_2^\mp$, the situation is somewhat more complicated. In order to extract the CP-odd parts of such processes, we need to form an asymmetry involving the two processes of eq. (8.6), and it will contain differences of the squared amplitudes of those two processes. The contributions from the tree-level diagrams alone will vanish, so to lowest order we expect to get contributions from the interference between the tree-level diagrams and one-loop diagrams (there are more one-loop diagrams than is shown in Fig. 12). We expect that this lowest-order contribution to the asymmetry can be written as a linear combination of the elements of the “linear algebraic basis” of CP-odd invariants J_i (more than 15).

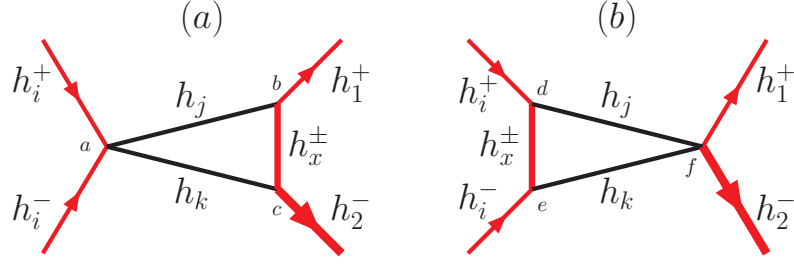


Figure 13: Loop diagrams contributing to $h_i^+ h_i^- \rightarrow h_1^+ h_2^-$. The couplings $a \dots f$ refer to the related process where all fields are incoming.

9 Scalar phenomenology

While details of the Yukawa sector would be relevant for a detailed model, there are several aspects of the scalar sector that are generic. We summarise here the most important features of the parameter points that are compatible with the imposed constraints.

9.1 Mass distributions

The different constraints remove the majority of the 2.8 million “raw” scan points of Refs. [2, 3], the remaining points are shown in blue and purple in fig. 14. Since the quartic couplings (λ s) are subject to the perturbativity constraints, and the coefficients of the bilinear terms are related to the λ s by the minimisation conditions, the masses are subject to an upper bound at the electroweak scale. Furthermore, the vicinity of the $U(1) \times U(1)$ symmetry favours low masses [3].

In this figure, the blue points satisfy a rather loose constraint on the electron EDM, $|d_e| < 10^{-27} e \cdot \text{cm}$, whereas the purple ones satisfy $|d_e| < 5 \cdot 10^{-29} e \cdot \text{cm}$. There is no obvious systematic difference between the two distributions. The mass ranges for the different states may be characterised as follows.

$h_2 = h_{\text{SM}}$:

$$m_{\text{ch}1} \in \{80 \text{ GeV}, \sim 300 \text{ GeV}\}, \quad m_{\text{ch}2} \in \{150 \text{ GeV}, \sim 400 \text{ GeV}\}, \quad (9.1a)$$

$$m_1 \in \{\sim 10 \text{ GeV}, m_{h_{\text{SM}}}\}, \quad m_3 \in \{m_{h_{\text{SM}}}, \sim 300 \text{ GeV}\}, \quad (9.1b)$$

$$m_4 \in \{\sim 250 \text{ GeV}, \sim 450 \text{ GeV}\}, \quad m_5 \in \{\sim 250 \text{ GeV}, \sim 500 \text{ GeV}\} \quad (9.1c)$$

$h_3 = h_{\text{SM}}$:

$$m_{\text{ch}1} \in \{80 \text{ GeV}, \sim 200 \text{ GeV}\}, \quad m_{\text{ch}2} \in \{150 \text{ GeV}, \sim 300 \text{ GeV}\}, \quad (9.2a)$$

$$m_1 \in \{\frac{1}{2} m_{h_{\text{SM}}}, \sim 90 \text{ GeV}\}, \quad m_2 \in \{\frac{1}{2} m_{h_{\text{SM}}}, m_{h_{\text{SM}}}\}, \quad (9.2b)$$

$$m_4 \in \{\sim 150 \text{ GeV}, \sim 300 \text{ GeV}\}, \quad m_5 \in \{\sim 200 \text{ GeV}, \sim 400 \text{ GeV}\} \quad (9.2c)$$

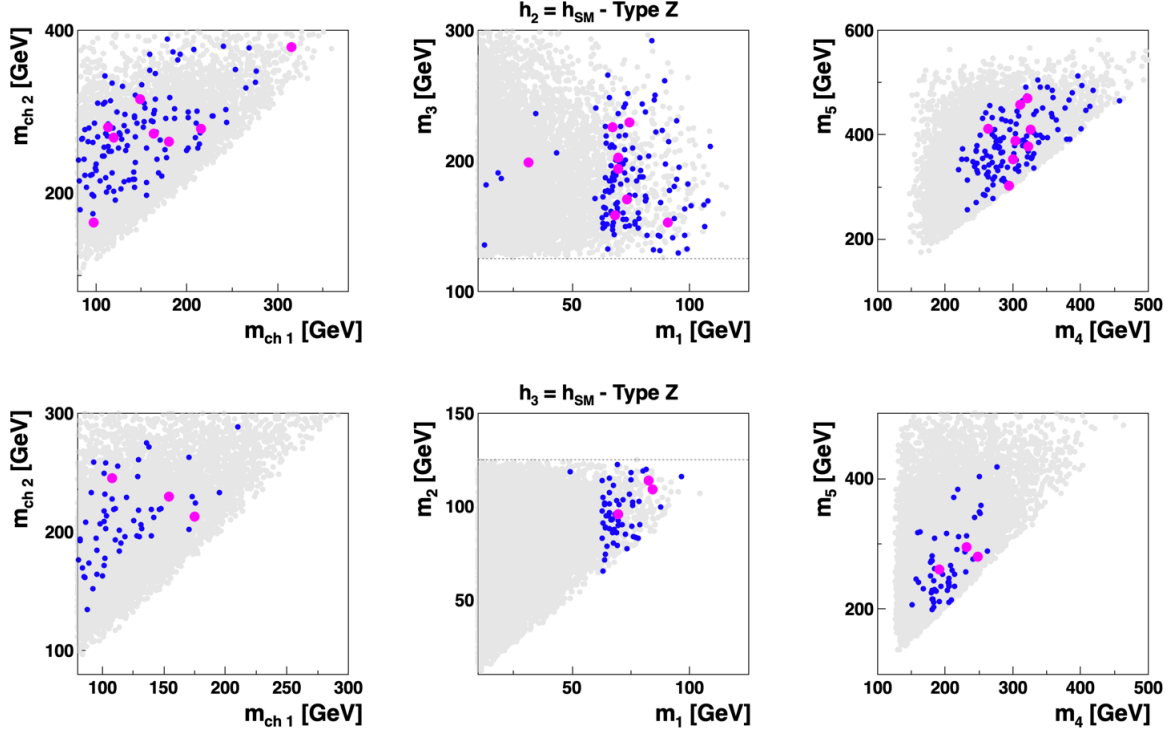


Figure 14: Scatter plots of allowed masses. Grey background: parameter points in the initial scan [2]; blue: parameter points satisfying all constraints for h_2 (top) or h_3 (bottom) identified as h_{SM} at 125 GeV. The (larger) purple points satisfy a stronger EDM constraint, $|d_e| < 5 \cdot 10^{-29} e \cdot \text{cm}$.

As a general feature we note that there are very few points with $m_1 < m_{h_{\text{SM}}}/2$. This holds both for $h_2 = h_{\text{SM}}$ and for $h_3 = h_{\text{SM}}$. Also, the very low values of the EDM (purple) are seemingly “randomly” distributed over these ranges.

9.2 Some θ distributions

We show in Fig. 15 scatter plots of scan points vs θ_2 and θ_3 (we recall that these are abbreviations for $\theta_2 - \theta_1$ and $\theta_3 - \theta_1$). As a reference, we display (black) histograms at the top showing the “input” distributions of scan points from Ref. [2]. Shown here are points for which h_2 or h_3 can be identified as the SM Higgs boson at 125 GeV. There are fewer points around $\theta_i = n\pi/2$. This is due to a depletion of these regions caused by the perturbativity constraints imposed on λ_2 and λ_3 . The way we solve the minimisation conditions, is to express λ_2 and λ_3 in terms of λ_1 , θ_2 and θ_3 . These constraints make λ_2 and λ_3 diverge for $\theta_i \rightarrow n\pi/2$.

However, there is a further depletion of these limits, which corresponds to CP conservation (see Appendix B), as illustrated by the blue points. These blue points show the ratio of two distributions: the parameter points surviving the constraints of (1) S , T , U

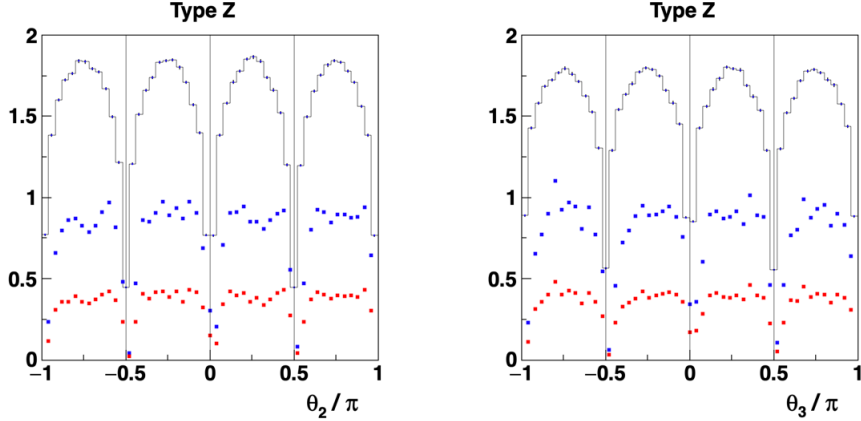


Figure 15: Scatter point distributions vs θ_2 and θ_3 . The (black) histograms at the top show the “input” distributions of scan points from Ref. [2]. There are fewer points at $\theta_i = n\pi/2$, since the minimisation conditions would force λ_2 and λ_3 to exceed the perturbativity bound in these limits. The blue points represent the ratios of points surviving the constraints of section 6, except for the EDM, normalized to the initial distribution. The red points show this same ratio, but restricted to parameter points for which $m_1 < 50$ GeV. The absolute normalizations contain no information.

(section 6.1), (2) $h_{\text{SM}} \rightarrow \gamma\gamma$ (section 6.2), (3) $\bar{B} \rightarrow X_s\gamma$ (section 6.3), divided by the input distribution shown in black at the top. While neither of these constraints refers to CP violation, there is a relative loss of points in the regions of CP conservation, as illustrated by the dips in the blue-point distributions.

This “loss of points” for θ_i near $n\pi/2$ is also seen in Fig. 16, where we show logarithms of the squared invariants vs θ_2 and θ_3 . This figure has some similarity to Fig. 1, except that we now have imposed all the discussed constraints. The grey points (“sums”) have all the discussed constraints imposed, except for the electron electric dipole moment. Likewise, the blue and yellow points refer to the “max” and “sum”, the latter excluding low masses. If we drop the constraint on m_1 , but require the electron EDM to be below $5 \cdot 10^{-29} e \cdot \text{cm}$ we obtain the purple points. Some values below $10^{-30} e \cdot \text{cm}$ were also encountered in the scan, as shown in Fig. 8.

It may be surprising that values of θ_2 and θ_3 well away from $n\pi/2$ are compatible with a small value of the electron EDM. A possible explanation is as follows. Suppose the EDM can be expanded in the CP-violating invariants,

$$d_e = \sum_{i=1}^{15} c_i J_i. \quad (9.3)$$

Then, without requiring the individual J_i to all be small, one could imagine cancellations among the 15 terms. See Eq. (4.5).

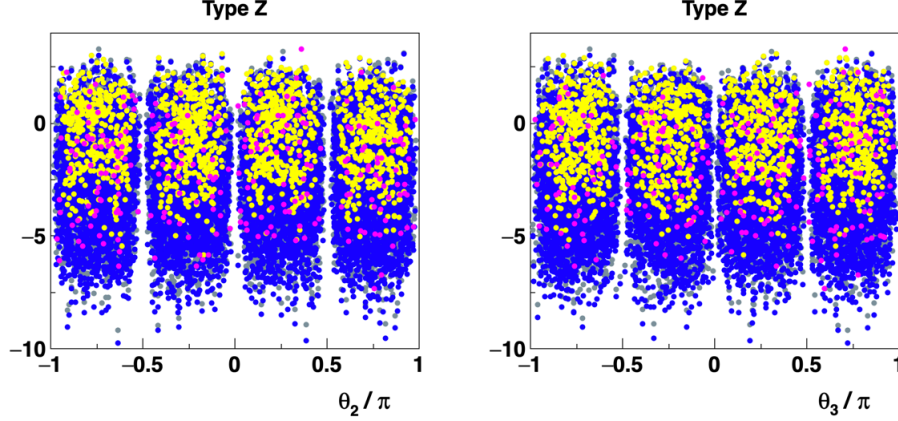


Figure 16: Scatter plots of logarithms of the sum and maxima of the squares of the 15 invariants. Grey: $\log_{10}(\sum_i |J_i^2|)$ (“sums”), blue: $\log_{10}(\max |J_i^2|)$ vs θ_2/π and θ_3/π . Yellow: “sums” for which $m_1 > 50$ GeV, purple: “sums” for which $|d_e| < 5 \cdot 10^{-29} e \cdot \text{cm}$.

9.3 Properties of the light states

A very important aspect of the Weinberg 3HDM potential is that, when requiring that some h_i has SM-like couplings to WW (and thus referred to as h_{SM}), then the potential tends to lead to one or two neutral states lighter than the h_{SM} [2, 3].

The light neutral scalars can be produced directly in pp collisions at the LHC (dominantly via gluon-gluon fusion), and also, if $m_1 < (m_j = m_{\text{SM}})/2$, by decay of the SM Higgs, $h_{\text{SM}} \rightarrow h_1 h_1$, at a rate given by

$$\Gamma = \frac{v^2}{32\pi m_j} |\hat{g}_{h_j h_1 h_1}|^2 \sqrt{1 - \frac{4m_1^2}{m_j^2}}, \quad (9.4)$$

where $h_j = h_{\text{SM}}$ and a factor of v has been extracted from the $h_j h_1 h_1$ coupling, $g = v\hat{g}$.

While it may be kinematically allowed for the SM Higgs candidate to decay to the lighter states, we must impose the condition that the rate for such decays does not exceed the invisible width, Γ_{inv} of the observed SM-like Higgs boson. According to the PDG [23], $\Gamma_{\text{inv}} < 0.19 \cdot \Gamma_{\text{tot}}$. The latter is however poorly determined, to $3.2^{+2.8}_{-2.2}$ MeV. We adopt the generous constraint $\Gamma_{\text{inv}} = 0.19 \times 6$ MeV, and require

$$h_3 = h_{\text{SM}} : \quad \Gamma(h_3 \rightarrow h_1 h_1) + \Gamma(h_3 \rightarrow h_2 h_1) < \Gamma_{\text{inv}}, \quad (9.5)$$

$$h_2 = h_{\text{SM}} : \quad \Gamma(h_2 \rightarrow h_1 h_1) < \Gamma_{\text{inv}}. \quad (9.6)$$

Light neutral scalars can not a priori be excluded, provided they only couple weakly [62–65].

Since the coupling to WW (and ZZ) is strongly suppressed, the h_i (lighter than h_{SM}) would dominantly decay to $b\bar{b}$ and $\tau\bar{\tau}$ with partial decay rates given by

$$\Gamma(h_i \rightarrow b\bar{b}) = \frac{3}{8\pi} m_i \left(\frac{m_b}{v}\right)^2 \beta \{ \beta^2 |\kappa_{h_i b\bar{b}}^S|^2 + |\kappa_{h_i b\bar{b}}^P|^2 \}, \quad (9.7a)$$

$$\Gamma(h_i \rightarrow \tau\bar{\tau}) = \frac{1}{8\pi} m_i \left(\frac{m_\tau}{v} \right)^2 \beta \{ \beta^2 |\kappa_{h_i\tau\bar{\tau}}^S|^2 + |\kappa_{h_i\tau\bar{\tau}}^P|^2 \}, \quad (9.7b)$$

where the couplings κ^S and κ^P are defined in Eq. (6.1). For Type Z Yukawa interactions the coupling modifiers κ for b -quarks and for τ -leptons will be independent.

In Fig. 17 we show the dominant decay width $\Gamma(h_i \rightarrow b\bar{b})$ as well as the approximate total width, $\Gamma(h_i \rightarrow b\bar{b}) + \Gamma(h_i \rightarrow \tau\bar{\tau})$ vs m_1 for the case when $h_2 = h_{\text{SM}}$. The total width is of the order 1–2 MeV, making a discovery of such decays very challenging.

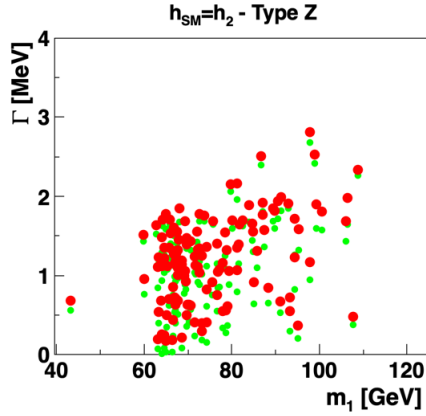


Figure 17: Scatter plots of decay widths $\Gamma(h_i \rightarrow b\bar{b})$ (green) and $\Gamma(h_i \rightarrow b\bar{b}) + \Gamma(h_i \rightarrow \tau\bar{\tau})$ (red) vs mass, for the lighter states, when $h_2 = h_{\text{SM}}$.

The Z boson cannot decay to a pair of identical spinless particles, whatever CP properties they might have. However, if also $m_2 < \frac{1}{2}m_Z$, then this mass region would be constrained by the Z width. Such decays would lead to final states like $h_1 h_2 \rightarrow b\bar{b}b\bar{b}$ and $h_1 h_2 \rightarrow b\bar{b}\tau\bar{\tau}$ with $m(f\bar{f}) < \frac{1}{2}m_Z$.

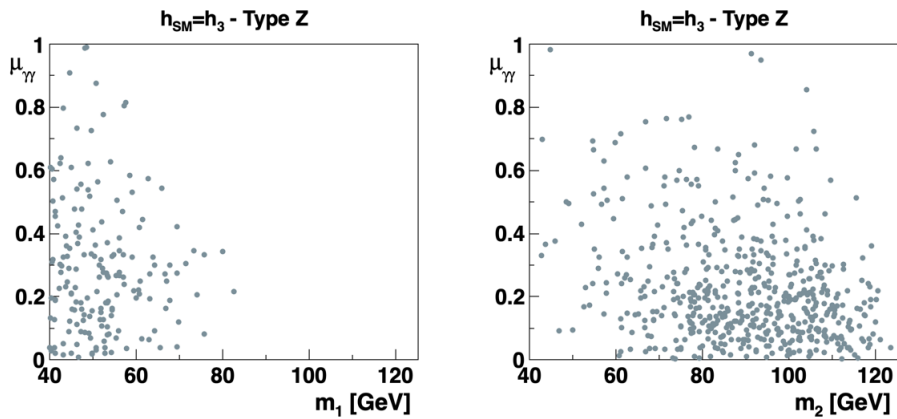


Figure 18: Scatter plots of relative digamma rate $\mu_{\gamma\gamma}$ vs mass, for the two lightest states, when $h_3 = h_{\text{SM}}$.

9.3.1 The 95 GeV mass region

CMS has noted the possibility of an excess in the digamma rates at an invariant mass of around 95 GeV [66]. This has recently been vigorously explored, in a 2HDM plus a real or complex singlet [67–73], in the related NMSSM [74], as well as in the 2HDM with unconventional Yukawa sectors [75, 76]. Several of these studies have also addressed the LEP excess in $b\bar{b}$ around the same energy [77, 78] and found it to be compatible with the model considered. More recently, also some excess in the $\tau^+\tau^-$ channel has been observed around the same mass [79] and analysed within the same framework [76, 80]. For an overview of these excesses, see Ref. [81], but it should also be noted that ATLAS does not see any excess [82, 83].

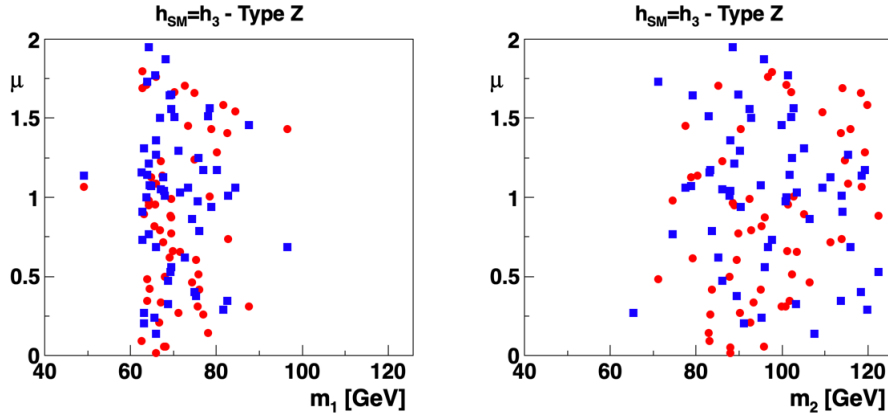


Figure 19: Scatter plots of signal strengths μ_{bb} (red bullets) and $\mu_{\tau\tau}$ (blue squares) vs mass, for the two lightest states, h_1 and h_2 , when $h_3 = h_{\text{SM}}$.

It is obviously of interest to see how the light neutral states of the Weinberg potential (those with mass below 125 GeV) compare with the claimed excesses. We show in Fig. 18 the digamma rate for $h_1 \rightarrow \gamma\gamma$ and $h_2 \rightarrow \gamma\gamma$, relative to the rate for an SM scalar at the same mass decaying to two photons. Here, “SM scalar” means that we calculate the digamma rate for a scalar at the considered mass, with couplings to fermions and the W the same as for the Standard Model. For h_2 with $m_2 = 95$ GeV there is clearly no problem in accommodating a value of the digamma signal strength, $\mu_{\gamma\gamma}$ around 0.2, as is suggested by the data.

Next, we turn to fermion final states. The light states will decay to $b\bar{b}$ and $\tau\bar{\tau}$ according to the Yukawa couplings given by Eq. (5.3). The relevant signal strengths will be given by

$$\mu_{h_i b\bar{b}} = (\kappa_{h_i b\bar{b}}^S)^2 + \frac{m_i^2}{m_i^2 - 4m_b^2} (\kappa_{h_i b\bar{b}}^P)^2, \quad (9.8)$$

and similarly for $\mu_{h_i \tau\bar{\tau}}$. We also show, in Fig. 19, the signal strength for $h_i \rightarrow b\bar{b}$ and $h_i \rightarrow \tau\bar{\tau}$, for h_1 and h_2 , assuming $h_3 = h_{\text{SM}}$. A wide range of values is populated, basically

from 0 up to 2, for the parameter points that are compatible with the constraints. The case $h_2 = h_{\text{SM}}$ is similar, but then obviously only h_1 is available as a “light” state.

It should also be stressed that, as compared with an SM-like scalar, the light scalars of the Weinberg potential have a much reduced decay width to $\gamma\gamma$, because of the reduced coupling, illustrated in fig. 4 of Ref. [2]. The dominant decay would be to $b\bar{b}$.

10 Concluding remarks

We have provided a full set of CP-odd invariants for the real Weinberg potential with complex vevs. Complex vevs normally signal CP violation. However, these invariants would all have to vanish for CP not to be violated. Thus, a full set of solutions is given, identifying limits in which they all vanish and CP is conserved.

Furthermore, we have illustrated some aspects of the phenomenology of this potential, which tends to yield two light CP-mixed states. Also, in spite of complex vevs, the potential is shown to be able to accommodate the recent low experimental upper bound on the electron electric dipole moment.

While our main focus has been on exhibiting mathematical features of the Weinberg 3HDM potential, it is clearly also of interest to ask how experimental data could support it or reject it. In particular, if one discovers an additional scalar, can one argue for the Weinberg 3HDM potential rather than some version of the 2HDM? Clearly, a light scalar (mass below 125 GeV) and strong couplings to Zh_{SM} are more naturally realised in the Weinberg 3HDM than in a 2HDM. Also, it should be noted that the Weinberg potential can lead to *two* light scalars, as well as at least one pair of light charged scalars.

Acknowledgements

We thank Robin Plantey and Marius A. Solberg for contributions to the early stages of this work. PO is supported in part by the Research Council of Norway. The work of MNR was partially supported by Fundação para a Ciência e a Tecnologia (FCT, Portugal) through the projects CFTP-FCT Unit UIDB/00777/2020 and UIDP/00777/2020, CERN/FIS-PAR/0002/2021, 2024.02004.CERN, which are partially funded through POCTI (FEDER), COMPETE, QREN and EU. We also thank CFTP/IST/University of Lisbon and the University of Bergen, where collaboration visits took place.

It is also a pleasure to thank Thomas Hahn for advice on the diagonalization of the mass matrices [84], as well as Mihail Misiak, Francesca Borzumati and Andreas Crivellin for discussions of the $\bar{B} \rightarrow X_s \gamma$ constraints.

A Mixing matrices in the Higgs basis

For some purposes the mixing matrices in the Higgs basis are very useful. We start by rewriting the neutral fields according to Eq. (4.6) of Ref. [2],

$$\begin{pmatrix} \eta_1 + i\chi_1 \\ \eta_2 + i\chi_2 \\ \eta_3 + i\chi_3 \end{pmatrix} = \tilde{R}^T \begin{pmatrix} \eta_1^{\text{HB}} + iG^0 \\ \eta_2^{\text{HB}} + i\chi_2^{\text{HB}} \\ \eta_3^{\text{HB}} + i\chi_3^{\text{HB}} \end{pmatrix}, \quad (\text{A.1})$$

where the η_i^{HB} and χ_i^{HB} refer to Higgs-basis fields, and (see Eq. (2.15) of Ref. [2])

$$\tilde{R} = \frac{1}{vw} \begin{pmatrix} |v_1|w & |v_2|w & |v_3|w \\ -w^2 & |v_1||v_2| & |v_1||v_3| \\ 0 & -|v_3|v & |v_2|v \end{pmatrix}, \quad (\text{A.2})$$

with $w^2 = v_2^2 + v_3^2$. Note that overall phases have been factored out in Eq. (2.1), where η_i and χ_i are defined. The Higgs-basis fields are related to the neutral mass eigenstates h_j by Eqs. (2.17) and (2.18) of Ref. [2], such that

$$\eta_1 = \sum_{i=1}^3 \tilde{R}_{i1} O_{ji} h_j, \quad \eta_2 = \sum_{i=1}^3 \tilde{R}_{i2} O_{ji} h_j, \quad \eta_3 = \sum_{i=1}^3 \tilde{R}_{i3} O_{ji} h_j, \quad (\text{A.3a})$$

$$\chi_1 = \sum_{i=2}^3 \tilde{R}_{i1} O_{j\,2+i} h_j, \quad \chi_2 = \sum_{i=2}^3 \tilde{R}_{i2} O_{j\,2+i} h_j, \quad \chi_3 = \sum_{i=2}^3 \tilde{R}_{i3} O_{j\,2+i} h_j. \quad (\text{A.3b})$$

Likewise, for the charged fields, we have from Eq. (A.2) of Ref. [2],

$$\varphi_1^+ = \sum_{i=2}^3 \tilde{R}_{i1} (U^\dagger)_{i-1\,j} h_j^+, \quad \varphi_2^+ = \sum_{i=2}^3 \tilde{R}_{i2} (U^\dagger)_{i-1\,j} h_j^+, \quad \varphi_3^+ = \sum_{i=2}^3 \tilde{R}_{i3} (U^\dagger)_{i-1\,j} h_j^+. \quad (\text{A.4})$$

The couplings of physical neutral states to ZZ or WW are given by the first column of the Higgs-basis rotation matrix which can be expressed in terms of \mathcal{O} ,

$$O_{i1} = \sum_{j=1}^3 \tilde{R}_{1j} \mathcal{O}_{i+1\,j} = \sum_{j=1}^3 \frac{v_j}{v} \mathcal{O}_{i+1\,j}. \quad (\text{A.5})$$

B CP-conserving limits

Let $\{i, j, k\}$ be any permutation of $\{1, 2, 3\}$. We shall in the following interpret $\lambda_{ij} = \lambda_{ji}$ and $\lambda'_{ij} = \lambda'_{ji}$ whenever $i > j$. We assume the most general form of the vevs, given by Eq. (3.1).

Below, we list all cases where CP is conserved, i.e., when Eq. (4.4) is satisfied, together with the solutions of the minimisation conditions. They will be ordered according to the number of vanishing vevs.

Furthermore, for all the presented cases, we shall also give the explicit form of the basis transformation that takes us to a real basis, i.e., a potential with only real parameters as well as real vevs. The transformation is of the form

$$\begin{pmatrix} \bar{\phi}_1 \\ \bar{\phi}_2 \\ \bar{\phi}_3 \end{pmatrix} = U \begin{pmatrix} \phi_1 \\ \phi_2 \\ \phi_3 \end{pmatrix}, \quad (\text{B.1})$$

and we present the matrix U for each case.

All the cases listed below are particular cases of the CP-conserving solutions presented in section 3.

B.1 Solutions with two vanishing vevs

$$v_i = 0, \quad v_j = 0, \quad m_{kk} = \lambda_{kk} v_k^2. \quad (\text{B.2})$$

$$U = \begin{pmatrix} e^{-i\theta_k} & 0 & 0 \\ 0 & e^{-i\theta_k} & 0 \\ 0 & 0 & e^{-i\theta_k} \end{pmatrix}, \quad \text{for } \{i, j, k\} = \{1, 2, 3\}. \quad (\text{B.3})$$

B.2 Solutions with one vanishing vev

There are seven cases. In addition to $v_i = 0$ they require

Case 1-1:

$$m_{jj} = \lambda_{jj} v_j^2 + \frac{1}{2} (\lambda'_{jk} + \lambda_{jk}) v_k^2, \quad (\text{B.4a})$$

$$m_{kk} = \lambda_{kk} v_k^2 + \frac{1}{2} (\lambda'_{jk} + \lambda_{jk}) v_j^2, \quad \lambda_i = \lambda_j = 0. \quad (\text{B.4b})$$

$$U = \begin{pmatrix} e^{-i\theta_j} & 0 & 0 \\ 0 & e^{-i\theta_j} & 0 \\ 0 & 0 & e^{-i\theta_k} \end{pmatrix}, \quad \text{for } \{i, j, k\} = \{1, 2, 3\}. \quad (\text{B.5})$$

Case 1-2:

$$m_{jj} = m_{kk} = \lambda_{jj} (v_j^2 + v_k^2), \quad \lambda_i = 0, \quad \lambda'_{ik} = \lambda'_{ij}, \quad \lambda_{ik} = \lambda_{ij}, \quad \lambda_{kk} = \lambda_{jj}, \quad (\text{B.6a})$$

$$\lambda_k = \lambda_j, \quad \lambda'_{jk} = 2\lambda_{jj} - \lambda_{jk}. \quad (\text{B.6b})$$

$$U = \begin{pmatrix} e^{i\alpha} & 0 & 0 \\ 0 & \frac{ie^{i(\alpha-\beta)}}{\sqrt{2}} & \frac{e^{i(\alpha-\beta)}}{\sqrt{2}} \\ 0 & -\frac{ie^{i(\alpha+\beta)}}{\sqrt{2}} & \frac{e^{i(\alpha+\beta)}}{\sqrt{2}} \end{pmatrix}, \quad \text{for } \{i, j, k\} = \{1, 2, 3\}. \quad (\text{B.7})$$

where

$$\alpha = \arctan \left(\frac{v_j^2 \cos 2\theta_j + v_k^2 \cos 2\theta_k - \sqrt{v_j^4 + v_k^4 + 2v_j^2 v_k^2 \cos 2(\theta_j - \theta_k)}}{v_j^2 \sin 2\theta_j + v_k^2 \sin 2\theta_k} \right), \quad (\text{B.8})$$

$$\beta = \arctan \left(\frac{v_j^2 - v_k^2 + \sqrt{v_j^4 + v_k^4 + 2v_j^2 v_k^2 \cos 2(\theta_j - \theta_k)}}{2v_j v_k \cos(\theta_j - \theta_k)} \right). \quad (\text{B.9})$$

Case 1-3:

$$m_{jj} = m_{kk} = \lambda_{jj} (v_j^2 + v_k^2), \quad \lambda_i = 0, \quad \lambda'_{ik} = \lambda'_{ij}, \quad \lambda_{ik} = \lambda_{ij}, \quad \lambda_{kk} = \lambda_{jj}, \quad (\text{B.10a})$$

$$\lambda_k = -\lambda_j, \quad \lambda'_{jk} = 2\lambda_{jj} - \lambda_{jk}. \quad (\text{B.10b})$$

$$U = \begin{pmatrix} e^{i\alpha} & 0 & 0 \\ 0 & \frac{e^{i(\alpha-\beta)}}{\sqrt{2}} & \frac{e^{i(\alpha-\beta)}}{\sqrt{2}} \\ 0 & -\frac{e^{i(\alpha+\beta)}}{\sqrt{2}} & \frac{e^{i(\alpha+\beta)}}{\sqrt{2}} \end{pmatrix}, \quad \text{for } \{i, j, k\} = \{1, 2, 3\}. \quad (\text{B.11})$$

where

$$\alpha = \arctan \left(\frac{v_j^2 \cos 2\theta_j - v_k^2 \cos 2\theta_k - \sqrt{v_j^4 + v_k^4 - 2v_j^2 v_k^2 \cos 2(\theta_j - \theta_k)}}{v_j^2 \sin 2\theta_j - v_k^2 \sin 2\theta_k} \right), \quad (\text{B.12})$$

$$\beta = \arctan \left(\frac{v_j^2 - v_k^2 - \sqrt{v_j^4 + v_k^4 - 2v_j^2 v_k^2 \cos 2(\theta_j - \theta_k)}}{2v_j v_k \sin(\theta_j - \theta_k)} \right). \quad (\text{B.13})$$

Case 1-4:

$$m_{jj} = m_{kk} = \frac{1}{2} (\lambda'_{jk} + 2\lambda_{jj} + \lambda_{jk}) v_j^2, \quad \lambda_i = 0, \quad \lambda'_{ik} = \lambda'_{ij}, \quad \lambda_{ik} = \lambda_{ij}, \quad (\text{B.14a})$$

$$\lambda_{kk} = \lambda_{jj}, \quad \lambda_k = \lambda_j, \quad v_k = v_j. \quad (\text{B.14b})$$

$$U = \begin{pmatrix} e^{-\frac{1}{2}i(\theta_j+\theta_k)} & 0 & 0 \\ 0 & \frac{1}{\sqrt{2}} & \frac{e^{-i(\theta_j+\theta_k)}}{\sqrt{2}} \\ 0 & -\frac{i}{\sqrt{2}} & \frac{ie^{-i(\theta_j+\theta_k)}}{\sqrt{2}} \end{pmatrix}, \quad \text{for } \{i, j, k\} = \{1, 2, 3\}. \quad (\text{B.15})$$

Case 1-5:

$$m_{jj} = m_{kk} = \frac{1}{2} (\lambda'_{jk} + 2\lambda_{jj} + \lambda_{jk}) v_j^2, \quad \lambda_i = 0, \quad \lambda'_{ik} = \lambda'_{ij}, \quad \lambda_{ik} = \lambda_{ij}, \quad (\text{B.16a})$$

$$\lambda_{kk} = \lambda_{jj}, \quad \lambda_k = -\lambda_j, \quad v_k = v_j. \quad (\text{B.16b})$$

$$U = \begin{pmatrix} e^{-\frac{1}{2}i(\theta_j+\theta_k-\frac{\pi}{2})} & 0 & 0 \\ 0 & \frac{e^{-\frac{1}{2}i(\theta_j+\theta_k)}}{\sqrt{2}} & \frac{e^{-\frac{1}{2}i(\theta_j+\theta_k)}}{\sqrt{2}} \\ 0 & -\frac{ie^{-\frac{1}{2}i(\theta_j+\theta_k)}}{\sqrt{2}} & \frac{ie^{-\frac{1}{2}i(\theta_j+\theta_k)}}{\sqrt{2}} \end{pmatrix}, \quad \text{for } \{i, j, k\} = \{1, 2, 3\}. \quad (\text{B.17})$$

Case 1-6:

$$m_{jj} = \lambda_{jj} v_j^2 + \frac{1}{2} (2\lambda_i + \lambda'_{jk} + \lambda_{jk}) v_k^2, \quad (\text{B.18a})$$

$$m_{kk} = \lambda_{kk} v_k^2 + \frac{1}{2} (2\lambda_i + \lambda'_{jk} + \lambda_{jk}) v_j^2, \quad \sin(\theta_k - \theta_j) = 0. \quad (\text{B.18b})$$

$$U = \begin{pmatrix} e^{-i\theta_j} & 0 & 0 \\ 0 & e^{-i\theta_j} & 0 \\ 0 & 0 & e^{-i\theta_j} \end{pmatrix}, \quad \text{for } \{i, j, k\} = \{1, 2, 3\}. \quad (\text{B.19})$$

Case 1-7:

$$m_{jj} = \lambda_{jj} v_j^2 + \frac{1}{2} (-2\lambda_i + \lambda'_{jk} + \lambda_{jk}) v_k^2, \quad (\text{B.20a})$$

$$m_{kk} = \lambda_{kk} v_k^2 + \frac{1}{2} (-2\lambda_i + \lambda'_{jk} + \lambda_{jk}) v_j^2, \quad \cos(\theta_k - \theta_j) = 0. \quad (\text{B.20b})$$

$$U = \begin{pmatrix} e^{-i\theta_j} & 0 & 0 \\ 0 & e^{-i\theta_j} & 0 \\ 0 & 0 & ie^{-i\theta_j} \end{pmatrix}, \quad \text{for } \{i, j, k\} = \{1, 2, 3\}. \quad (\text{B.21})$$

B.3 Solutions with no vanishing vev

With all three vevs non-zero, there are 11 cases of CP conservation. They all require special values of the angles, or the vanishing of couplings sensitive to the angles:

Case 0-1:

$$m_{11} = \lambda_{11} v_1^2 + \frac{1}{2} (2\lambda_3 + \lambda'_{12} + \lambda_{12}) v_2^2 + \frac{1}{2} (2\lambda_2 + \lambda'_{13} + \lambda_{13}) v_3^2, \quad (\text{B.22a})$$

$$m_{22} = \lambda_{22} v_2^2 + \frac{1}{2} (2\lambda_3 + \lambda'_{12} + \lambda_{12}) v_1^2 + \frac{1}{2} (2\lambda_1 + \lambda'_{23} + \lambda_{23}) v_3^2, \quad (\text{B.22b})$$

$$m_{33} = \lambda_{33} v_3^2 + \frac{1}{2} (2\lambda_2 + \lambda'_{13} + \lambda_{13}) v_1^2 + \frac{1}{2} (2\lambda_1 + \lambda'_{23} + \lambda_{23}) v_2^2, \quad (\text{B.22c})$$

$$\sin(\theta_2 - \theta_1) = \sin(\theta_3 - \theta_1) = 0. \quad (\text{B.22d})$$

$$U = \begin{pmatrix} e^{-i\theta_1} & 0 & 0 \\ 0 & e^{-i\theta_1} & 0 \\ 0 & 0 & e^{-i\theta_1} \end{pmatrix} \quad (\text{B.23})$$

Case 0-2:

$$m_{11} = \lambda_{11} v_1^2 + \frac{1}{2} (2\lambda_3 + \lambda'_{12} + \lambda_{12}) v_2^2 + \frac{1}{2} (-2\lambda_2 + \lambda'_{13} + \lambda_{13}) v_3^2, \quad (\text{B.24a})$$

$$m_{22} = \lambda_{22} v_2^2 + \frac{1}{2} (2\lambda_3 + \lambda'_{12} + \lambda_{12}) v_1^2 + \frac{1}{2} (-2\lambda_1 + \lambda'_{23} + \lambda_{23}) v_3^2, \quad (\text{B.24b})$$

$$m_{33} = \lambda_{33} v_3^2 + \frac{1}{2} (-2\lambda_2 + \lambda'_{13} + \lambda_{13}) v_1^2 + \frac{1}{2} (-2\lambda_1 + \lambda'_{23} + \lambda_{23}) v_2^2, \quad (\text{B.24c})$$

$$\sin(\theta_2 - \theta_1) = \cos(\theta_3 - \theta_1) = 0. \quad (\text{B.24d})$$

$$U = \begin{pmatrix} e^{-i\theta_1} & 0 & 0 \\ 0 & e^{-i\theta_1} & 0 \\ 0 & 0 & ie^{-i\theta_1} \end{pmatrix} \quad (\text{B.25})$$

Case 0-3:

$$m_{11} = \lambda_{11}v_1^2 + \frac{1}{2}(-2\lambda_3 + \lambda'_{12} + \lambda_{12})v_2^2 + \frac{1}{2}(2\lambda_2 + \lambda'_{13} + \lambda_{13})v_3^2, \quad (\text{B.26a})$$

$$m_{22} = \lambda_{22}v_2^2 + \frac{1}{2}(-2\lambda_3 + \lambda'_{12} + \lambda_{12})v_1^2 + \frac{1}{2}(-2\lambda_1 + \lambda'_{23} + \lambda_{23})v_3^2, \quad (\text{B.26b})$$

$$m_{33} = \lambda_{33}v_3^2 + \frac{1}{2}(2\lambda_2 + \lambda'_{13} + \lambda_{13})v_1^2 + \frac{1}{2}(-2\lambda_1 + \lambda'_{23} + \lambda_{23})v_2^2, \quad (\text{B.26c})$$

$$\cos(\theta_2 - \theta_1) = \sin(\theta_3 - \theta_1) = 0. \quad (\text{B.26d})$$

$$U = \begin{pmatrix} e^{-i\theta_1} & 0 & 0 \\ 0 & ie^{-i\theta_1} & 0 \\ 0 & 0 & e^{-i\theta_1} \end{pmatrix} \quad (\text{B.27})$$

Case 0-4:

$$m_{11} = \lambda_{11}v_1^2 + \frac{1}{2}(-2\lambda_3 + \lambda'_{12} + \lambda_{12})v_2^2 + \frac{1}{2}(-2\lambda_2 + \lambda'_{13} + \lambda_{13})v_3^2, \quad (\text{B.28a})$$

$$m_{22} = \lambda_{22}v_2^2 + \frac{1}{2}(-2\lambda_3 + \lambda'_{12} + \lambda_{12})v_1^2 + \frac{1}{2}(2\lambda_1 + \lambda'_{23} + \lambda_{23})v_3^2, \quad (\text{B.28b})$$

$$m_{33} = \lambda_{33}v_3^2 + \frac{1}{2}(-2\lambda_2 + \lambda'_{13} + \lambda_{13})v_1^2 + \frac{1}{2}(2\lambda_1 + \lambda'_{23} + \lambda_{23})v_2^2, \quad (\text{B.28c})$$

$$\cos(\theta_2 - \theta_1) = \cos(\theta_3 - \theta_1) = 0. \quad (\text{B.28d})$$

$$U = \begin{pmatrix} e^{-i\theta_1} & 0 & 0 \\ 0 & ie^{-i\theta_1} & 0 \\ 0 & 0 & ie^{-i\theta_1} \end{pmatrix} \quad (\text{B.29})$$

Case 0-5:

$$m_{ii} = \lambda_{ii}v_i^2 + \frac{1}{2}(\lambda'_{ij} + \lambda_{ij})v_j^2 + \frac{1}{2}(\lambda'_{ik} + \lambda_{ik})v_k^2, \quad (\text{B.30a})$$

$$m_{jj} = \lambda_{jj}v_j^2 + \frac{1}{2}(\lambda'_{ij} + \lambda_{ij})v_i^2 + \frac{1}{2}(2\lambda_i + \lambda'_{jk} + \lambda_{jk})v_k^2, \quad (\text{B.30b})$$

$$m_{kk} = \lambda_{kk}v_k^2 + \frac{1}{2}(\lambda'_{ik} + \lambda_{ik})v_i^2 + \frac{1}{2}(2\lambda_i + \lambda'_{jk} + \lambda_{jk})v_j^2, \quad (\text{B.30c})$$

$$\lambda_k = \lambda_j = 0, \quad \sin(\theta_k - \theta_j) = 0. \quad (\text{B.30d})$$

$$U = \begin{pmatrix} e^{-i\theta_i} & 0 & 0 \\ 0 & e^{-i\theta_j} & 0 \\ 0 & 0 & e^{-i\theta_j} \end{pmatrix}, \quad \text{for } \{i, j, k\} = \{1, 2, 3\}. \quad (\text{B.31})$$

Case 0-6:

$$m_{ii} = \lambda_{ii} v_i^2 + \frac{1}{2} (\lambda'_{ij} + \lambda_{ij}) v_j^2 + \frac{1}{2} (\lambda'_{ik} + \lambda_{ik}) v_k^2, \quad (\text{B.32a})$$

$$m_{jj} = \lambda_{jj} v_j^2 + \frac{1}{2} (\lambda'_{ij} + \lambda_{ij}) v_i^2 + \frac{1}{2} (-2\lambda_i + \lambda'_{jk} + \lambda_{jk}) v_k^2, \quad (\text{B.32b})$$

$$m_{kk} = \lambda_{kk} v_k^2 + \frac{1}{2} (\lambda'_{ik} + \lambda_{ik}) v_i^2 + \frac{1}{2} (-2\lambda_i + \lambda'_{jk} + \lambda_{jk}) v_j^2, \quad (\text{B.32c})$$

$$\lambda_k = \lambda_j = 0, \quad \cos(\theta_k - \theta_j) = 0. \quad (\text{B.32d})$$

$$U = \begin{pmatrix} e^{-i\theta_i} & 0 & 0 \\ 0 & e^{-i\theta_j} & 0 \\ 0 & 0 & ie^{-i\theta_j} \end{pmatrix}, \quad \text{for } \{i, j, k\} = \{1, 2, 3\}. \quad (\text{B.33})$$

Case 0-7:

$$m_{11} = \lambda_{11} v_1^2 + \frac{1}{2} (\lambda'_{12} + \lambda_{12}) v_2^2 + \frac{1}{2} (\lambda'_{13} + \lambda_{13}) v_3^2, \quad (\text{B.34a})$$

$$m_{22} = \lambda_{22} v_2^2 + \frac{1}{2} (\lambda'_{12} + \lambda_{12}) v_1^2 + \frac{1}{2} (\lambda'_{23} + \lambda_{23}) v_3^2, \quad (\text{B.34b})$$

$$m_{33} = \lambda_{33} v_3^2 + \frac{1}{2} (\lambda'_{13} + \lambda_{13}) v_1^2 + \frac{1}{2} (\lambda'_{23} + \lambda_{23}) v_2^2, \quad (\text{B.34c})$$

$$\lambda_3 = \lambda_2 = \lambda_1 = 0. \quad (\text{B.34d})$$

$$U = \begin{pmatrix} e^{-i\theta_1} & 0 & 0 \\ 0 & e^{-i\theta_2} & 0 \\ 0 & 0 & e^{-i\theta_3} \end{pmatrix} \quad (\text{B.35})$$

Case 0-8:

$$m_{ii} = \lambda_{ii} v_i^2 + \frac{1}{2} (\lambda'_{ij} + \lambda_{ij}) \left(1 + \frac{\sin 2(\theta_i - \theta_j)}{\sin 2(\theta_i - \theta_k)} \right) v_j^2 + \frac{\lambda_i v_j^4 \sin^2 2(\theta_j - \theta_k)}{v_i^2 \sin^2 2(\theta_i - \theta_k)}, \quad (\text{B.36a})$$

$$m_{jj} = m_{kk} = (\lambda_{jj} + \lambda_i) \left(1 + \frac{\sin 2(\theta_i - \theta_j)}{\sin 2(\theta_i - \theta_k)} \right) v_j^2 + \frac{1}{2} (\lambda'_{ij} + \lambda_{ij}) v_i^2, \quad (\text{B.36b})$$

$$\lambda_k = -\lambda_j = \frac{\lambda_i v_j^2 \sin 2(\theta_j - \theta_k)}{v_i^2 \sin 2(\theta_i - \theta_k)}, \quad \lambda'_{ik} = \lambda'_{ij}, \quad \lambda_{ik} = \lambda_{ij}, \quad \lambda_{kk} = \lambda_{jj}, \quad (\text{B.36c})$$

$$v_k^2 = v_j^2 \frac{\sin 2(\theta_i - \theta_j)}{\sin 2(\theta_i - \theta_k)}, \quad \lambda'_{jk} = 2\lambda_i + 2\lambda_{jj} - \lambda_{jk}. \quad (\text{B.36d})$$

$$U = \begin{pmatrix} e^{-i\theta_i} & 0 & 0 \\ 0 & e^{-i\theta_j} \cos \alpha & e^{-i\theta_k} \sin \alpha \\ 0 & -e^{i(\theta_k - 2\theta_i)} \sin \alpha & e^{i(\theta_j - 2\theta_i)} \cos \alpha \end{pmatrix}, \quad \text{for } \{i, j, k\} = \{1, 2, 3\}, \quad (\text{B.37})$$

where

$$\alpha = \arctan \sqrt{\frac{\sin 2(\theta_i - \theta_j)}{\sin 2(\theta_i - \theta_k)}} = \arctan \left(\frac{v_k}{v_j} \right). \quad (\text{B.38})$$

Case 0-9:

$$m_{ii} = \lambda_{ii} v_i^2 + \frac{1}{2} (\lambda'_{ij} + \lambda_{ij}) \left(1 - \frac{\sin 2(\theta_i - \theta_j)}{\sin 2(\theta_i - \theta_k)} \right) v_j^2 - \frac{\lambda_i v_j^4 \sin^2 2(\theta_j - \theta_k)}{v_i^2 \sin^2 2(\theta_i - \theta_k)}, \quad (\text{B.39a})$$

$$m_{jj} = m_{kk} = (\lambda_{jj} - \lambda_i) \left(1 - \frac{\sin 2(\theta_i - \theta_j)}{\sin 2(\theta_i - \theta_k)} \right) v_j^2 + \frac{1}{2} (\lambda'_{ij} + \lambda_{ij}) v_i^2, \quad (\text{B.39b})$$

$$\lambda_k = \lambda_j = -\frac{\lambda_i v_j^2 \sin 2(\theta_j - \theta_k)}{v_i^2 \sin 2(\theta_i - \theta_k)}, \quad \lambda'_{ik} = \lambda'_{ij}, \quad \lambda_{ik} = \lambda_{ij}, \quad \lambda_{kk} = \lambda_{jj}, \quad (\text{B.39c})$$

$$v_k^2 = -v_j^2 \frac{\sin 2(\theta_i - \theta_j)}{\sin 2(\theta_i - \theta_k)}, \quad \lambda'_{jk} = -2\lambda_i + 2\lambda_{jj} - \lambda_{jk}. \quad (\text{B.39d})$$

$$U = \begin{pmatrix} e^{-i\theta_i} & 0 & 0 \\ 0 & e^{-i\theta_j} \cos \alpha & e^{-i\theta_k} \sin \alpha \\ 0 & -ie^{i(\theta_k - 2\theta_i)} \sin \alpha & ie^{i(\theta_j - 2\theta_i)} \cos \alpha \end{pmatrix}, \quad \text{for } \{i, j, k\} = \{1, 2, 3\}, \quad (\text{B.40})$$

where

$$\alpha = \arctan \sqrt{-\frac{\sin 2(\theta_i - \theta_j)}{\sin 2(\theta_i - \theta_k)}} = \arctan \left(\frac{v_k}{v_j} \right). \quad (\text{B.41})$$

Case 0-10:

$$m_{ii} = \lambda_{ii} v_i^2 + (\lambda'_{ij} + \lambda_{ij}) v_j^2 + \frac{4\lambda_i v_j^4 \cos^2 2(\theta_i - \theta_j)}{v_i^2}, \quad (\text{B.42a})$$

$$m_{jj} = m_{kk} = (\lambda_{jj} + \lambda_i) v_j^2 + \frac{1}{2} (\lambda'_{ij} + \lambda_{ij}) v_i^2 + \frac{1}{2} (\lambda'_{jk} + \lambda_{jk}) v_j^2, \quad (\text{B.42b})$$

$$\lambda_k = -\lambda_j = \frac{2\lambda_i v_j^2 \cos 2(\theta_i - \theta_j)}{v_i^2}, \quad (\text{B.42c})$$

$$\lambda'_{ik} = \lambda'_{ij}, \quad \lambda_{ik} = \lambda_{ij}, \quad \lambda_{kk} = \lambda_{jj}, \quad v_k = v_j, \quad (\text{B.42d})$$

$$\cos(2\theta_i - \theta_j - \theta_k) = 0, \quad \sin(2\theta_i - \theta_j - \theta_k) = \pm 1. \quad (\text{B.42e})$$

$$U = e^{-i\theta_i} \begin{pmatrix} 1 & 0 & 0 \\ 0 & \pm \frac{i}{\sqrt{2}} & \frac{1}{\sqrt{2}} \\ 0 & \pm \frac{1}{\sqrt{2}} & \frac{i}{\sqrt{2}} \end{pmatrix}, \quad \text{for } \{i, j, k\} = \{1, 2, 3\}. \quad (\text{B.43})$$

Case 0-11:

$$m_{ii} = \lambda_{ii} v_i^2 + (\lambda'_{ij} + \lambda_{ij}) v_j^2 - \frac{4\lambda_i v_j^4 \cos^2 2(\theta_i - \theta_j)}{v_i^2}, \quad (\text{B.44a})$$

$$m_{jj} = m_{kk} = (\lambda_{jj} - \lambda_i) v_j^2 + \frac{1}{2} (\lambda'_{ij} + \lambda_{ij}) v_i^2 + \frac{1}{2} (\lambda'_{jk} + \lambda_{jk}) v_j^2, \quad (\text{B.44b})$$

$$\lambda_k = \lambda_j = -\frac{2\lambda_i v_j^2 \cos 2(\theta_i - \theta_j)}{v_i^2}, \quad (\text{B.44c})$$

$$\lambda'_{ik} = \lambda'_{ij}, \quad \lambda_{ik} = \lambda_{ij}, \quad \lambda_{kk} = \lambda_{jj}, \quad v_k = v_j, \quad (\text{B.44d})$$

$$\sin(2\theta_i - \theta_j - \theta_k) = 0, \quad \cos(2\theta_i - \theta_j - \theta_k) = \pm 1. \quad (\text{B.44e})$$

$$U = e^{-i\theta_i} \begin{pmatrix} 1 & 0 & 0 \\ 0 & \pm \frac{1}{\sqrt{2}} & \frac{1}{\sqrt{2}} \\ 0 & \mp \frac{i}{\sqrt{2}} & \frac{i}{\sqrt{2}} \end{pmatrix}, \quad \text{for } \{i, j, k\} = \{1, 2, 3\}. \quad (\text{B.45})$$

This last case corresponds to the “simple model” of ref. [2].

C Invariants require two \hat{V} factors

The CP-odd invariants discussed in section 4 involve at least *two* factors \hat{V} . For a real potential invariants with just one such factor vanish. The imaginary part of \hat{V}_{ac} is antisymmetric in the indices a and c . However, with potential coefficients that are subject to the $\mathbb{Z}_2 \times \mathbb{Z}_2$ symmetry there is no way to construct an antisymmetric tensor F_{ca} that could project out this imaginary part. While there could be many different Z couplings, some are equal and some vanish. In the Weinberg potential, we have only four patterns of indices for which the Z_{acbd} can be non-zero:

$$Z_{iiii} = \lambda_{ii}, \quad Z_{iijj} = \lambda_{ij}, \quad Z_{ijji} = \lambda'_{ij}, \quad Z_{ijij} = \lambda_k. \quad (\text{C.1})$$

These all have pairs of repeated indices.

With two factors \hat{V}_{ac} and \hat{V}_{be} one can construct an imaginary quantity that is symmetric under two pairs of indices, $a \leftrightarrow b$ and $c \leftrightarrow e$, proportional to

$$\cos(\theta_a - \theta_c) \sin(\theta_b - \theta_e) + \cos(\theta_b - \theta_e) \sin(\theta_a - \theta_c). \quad (\text{C.2})$$

For $a = b$ and $c = e$, this is simply $\sin 2(\theta_a - \theta_c)$. This can for example be multiplied by a product of Z 's involving a factor $(Z_{aaaa} - Z_{cccc}) = 2(\lambda_{aa} - \lambda_{cc})$, or $(Z_{aadd} - Z_{ccdd}) = \lambda_{ad} - \lambda_{cd}$, see Eq. (4.5). The relative sign arises from rewriting

$$\sin 2(\theta_c - \theta_a) = -\sin 2(\theta_a - \theta_c). \quad (\text{C.3})$$

D 3HDM gauge coupling relations

As mentioned in section 8.1, there exist relations between the gauge-gauge-scalar couplings e_i and the gauge-scalar-scalar couplings λ_{ij} . In the 2HDM they are very simple [14], whereas in the 3HDM they are more involved.

In order to form a set of independent gauge couplings let us first pick the set of e_1, e_2, e_3, e_4, e_5 which are all independent. Next, by applying identities derived from the orthogonality of the rotation matrix we find that

$$\lambda_{12} = \frac{-e_5 \lambda_{34} + e_4 \lambda_{35} - e_3 \lambda_{45}}{v}, \quad (\text{D.1})$$

$$\lambda_{13} = \frac{(e_1 e_4 v - e_2 e_3 e_5) \lambda_{34} + (e_1 e_5 v + e_2 e_3 e_4) \lambda_{35} + e_2 (v^2 - e_3^2) \lambda_{45}}{(e_1^2 + e_2^2) v}, \quad (\text{D.2})$$

$$\lambda_{14} = \frac{-(e_1 e_3 v + e_2 e_4 e_5) \lambda_{34} - e_2 (v^2 - e_4^2) \lambda_{35} + (e_1 e_5 v - e_2 e_3 e_4) \lambda_{45}}{(e_1^2 + e_2^2) v}, \quad (\text{D.3})$$

$$\lambda_{15} = \frac{e_2 (v^2 - e_5^2) \lambda_{34} + (e_2 e_4 e_5 - e_1 e_3 v) \lambda_{35} - (e_1 e_4 v + e_2 e_3 e_5) \lambda_{45}}{(e_1^2 + e_2^2) v}, \quad (\text{D.4})$$

$$\lambda_{23} = \frac{(e_2 e_4 v + e_1 e_3 e_5) \lambda_{34} + (e_2 e_5 v - e_1 e_3 e_4) \lambda_{35} - e_1 (v^2 - e_3^2) \lambda_{45}}{(e_1^2 + e_2^2) v}, \quad (\text{D.5})$$

$$\lambda_{24} = \frac{(e_1 e_4 e_5 - e_2 e_3 v) \lambda_{34} + e_1 (v^2 - e_4^2) \lambda_{35} + (e_2 e_5 v + e_1 e_3 e_4) \lambda_{45}}{(e_1^2 + e_2^2) v}, \quad (\text{D.6})$$

$$\lambda_{25} = -\frac{e_1 (v^2 - e_5^2) \lambda_{34} + (e_2 e_3 v + e_1 e_4 e_5) \lambda_{35} + (e_2 e_4 v - e_1 e_3 e_5) \lambda_{45}}{(e_1^2 + e_2^2) v}. \quad (\text{D.7})$$

Hence, all gauge couplings involving neutral scalars can be expressed in terms of $e_1, e_2, e_3, e_4, e_5, \lambda_{34}, \lambda_{35}$ and λ_{45} , a total of eight couplings.

Finally, using

$$\begin{aligned} & (v^2 - e_5^2) \lambda_{34}^2 + (v^2 - e_4^2) \lambda_{35}^2 + (v^2 - e_3^2) \lambda_{45}^2 \\ & + 2e_4 e_5 \lambda_{34} \lambda_{35} - 2e_3 e_5 \lambda_{34} \lambda_{45} + 2e_3 e_4 \lambda_{35} \lambda_{45} - (e_1^2 + e_2^2) v^2 = 0. \end{aligned} \quad (\text{D.8})$$

we may bring the number of independent couplings down to seven by solving this quadratic equation for λ_{34} , λ_{35} or λ_{45} .

References

- [1] S. Weinberg, *Gauge Theory of CP Violation*, *Phys. Rev. Lett.* **37** (1976) 657.
- [2] R. Plantey, O. M. Ogreid, P. Osland, M. N. Rebelo and M. A. Solberg, *Weinberg's 3HDM potential with spontaneous CP violation*, *Phys. Rev. D* **108** (2023) 075029, [2208.13594].
- [3] R. Plantey, O. M. Ogreid, P. Osland, M. N. Rebelo and M. A. Solberg, *Light scalars in the Weinberg 3HDM potential with spontaneous CP violation*, *PoS DISCRETE2020-2021* (2022) 064, [2209.06499].
- [4] I. P. Ivanov and C. C. Nishi, *Symmetry breaking patterns in 3HDM*, *JHEP* **01** (2015) 021, [1410.6139].
- [5] G. C. Branco, *Spontaneous CP Nonconservation and Natural Flavor Conservation: A Minimal Model*, *Phys. Rev. D* **22** (1980) 2901.
- [6] G. C. Branco, L. Lavoura and J. P. Silva, *CP Violation*, vol. 103. Oxford University Press, 1999.

- [7] A. Mendez and A. Pomarol, *Signals of CP violation in the Higgs sector*, *Phys. Lett. B* **272** (1991) 313–318.
- [8] L. Lavoura and J. P. Silva, *Fundamental CP violating quantities in a $SU(2) \times U(1)$ model with many Higgs doublets*, *Phys. Rev. D* **50** (1994) 4619–4624, [[hep-ph/9404276](#)].
- [9] F. J. Botella and J. P. Silva, *Jarlskog - like invariants for theories with scalars and fermions*, *Phys. Rev. D* **51** (1995) 3870–3875, [[hep-ph/9411288](#)].
- [10] G. C. Branco, M. N. Rebelo and J. I. Silva-Marcos, *CP-odd invariants in models with several Higgs doublets*, *Phys. Lett. B* **614** (2005) 187–194, [[hep-ph/0502118](#)].
- [11] J. F. Gunion and H. E. Haber, *Conditions for CP-violation in the general two-Higgs-doublet model*, *Phys. Rev. D* **72** (2005) 095002, [[hep-ph/0506227](#)].
- [12] S. Davidson and H. E. Haber, *Basis-independent methods for the two-Higgs-doublet model*, *Phys. Rev. D* **72** (2005) 035004, [[hep-ph/0504050](#)].
- [13] H. E. Haber and D. O’Neil, *Basis-independent methods for the two-Higgs-doublet model. II. The Significance of $\tan\beta$* , *Phys. Rev. D* **74** (2006) 015018, [[hep-ph/0602242](#)].
- [14] B. Grzadkowski, O. M. Ogreid and P. Osland, *Measuring CP violation in Two-Higgs-Doublet models in light of the LHC Higgs data*, *JHEP* **11** (2014) 084, [[1409.7265](#)].
- [15] B. Grzadkowski, O. M. Ogreid and P. Osland, *Spontaneous CP violation in the 2HDM: physical conditions and the alignment limit*, *Phys. Rev. D* **94** (2016) 115002, [[1609.04764](#)].
- [16] W. R. Inc., “Mathematica.”
- [17] J. Hernandez-Sanchez, V. Keus, S. Moretti, D. Rojas-Ciofalo and D. Sokolowska, *Complementary Probes of Two-component Dark Matter*, [2012.11621](#).
- [18] J. Hernandez-Sanchez, V. Keus, S. Moretti and D. Sokolowska, *Complementary collider and astrophysical probes of multi-component Dark Matter*, *JHEP* **03** (2023) 045, [[2202.10514](#)].
- [19] R. Boto, P. N. Figueiredo, J. C. Romão and J. P. Silva, *Novel two component dark matter features in the $Z_2 \times Z_2$ 3HDM*, [2407.15933](#).
- [20] F. Borzumati and C. Greub, *2HDMs predictions for $\text{anti-}B \rightarrow X(s)$ gamma in NLO QCD*, *Phys. Rev. D* **58** (1998) 074004, [[hep-ph/9802391](#)].

- [21] M. Ciuchini, G. Degrandi, P. Gambino and G. Giudice, *Next-to-leading QCD corrections to $B \rightarrow X_s \gamma$: Standard model and two Higgs doublet model*, *Nucl. Phys. B* **527** (1998) 21–43, [[hep-ph/9710335](#)].
- [22] T. Hermann, M. Misiak and M. Steinhauser, *$\bar{B} \rightarrow X_s \gamma$ in the Two Higgs Doublet Model up to Next-to-Next-to-Leading Order in QCD*, *JHEP* **11** (2012) 036, [[1208.2788](#)].
- [23] PARTICLE DATA GROUP collaboration, R. L. Workman et al., *Review of Particle Physics*, *PTEP* **2022** (2022) 083C01.
- [24] CMS collaboration, A. Tumasyan et al., *Analysis of the CP structure of the Yukawa coupling between the Higgs boson and τ leptons in proton-proton collisions at $\sqrt{s} = 13$ TeV*, *JHEP* **06** (2022) 012, [[2110.04836](#)].
- [25] M. E. Peskin and T. Takeuchi, *A New constraint on a strongly interacting Higgs sector*, *Phys. Rev. Lett.* **65** (1990) 964–967.
- [26] M. E. Peskin and T. Takeuchi, *Estimation of oblique electroweak corrections*, *Phys. Rev. D* **46** (1992) 381–409.
- [27] I. Maksymyk, C. P. Burgess and D. London, *Beyond S, T and U*, *Phys. Rev. D* **50** (1994) 529–535, [[hep-ph/9306267](#)].
- [28] W. Grimus, L. Lavoura, O. M. Ogreid and P. Osland, *A Precision constraint on multi-Higgs-doublet models*, *J. Phys. G* **35** (2008) 075001, [[0711.4022](#)].
- [29] W. Grimus, L. Lavoura, O. M. Ogreid and P. Osland, *The Oblique parameters in multi-Higgs-doublet models*, *Nucl. Phys. B* **801** (2008) 81–96, [[0802.4353](#)].
- [30] P. Asadi, C. Cesarotti, K. Fraser, S. Homiller and A. Parikh, *Oblique lessons from the W-mass measurement at CDF II*, *Phys. Rev. D* **108** (2023) 055026, [[2204.05283](#)].
- [31] J. R. Ellis, M. K. Gaillard and D. V. Nanopoulos, *A Phenomenological Profile of the Higgs Boson*, *Nucl. Phys. B* **106** (1976) 292.
- [32] M. A. Shifman, A. Vainshtein, M. Voloshin and V. I. Zakharov, *Low-Energy Theorems for Higgs Boson Couplings to Photons*, *Sov. J. Nucl. Phys.* **30** (1979) 711–716.
- [33] J. F. Gunion, H. E. Haber, G. L. Kane and S. Dawson, *The Higgs Hunter’s Guide*, vol. 80. Frontiers in Physics, 2000.
- [34] A. Djouadi, *The Anatomy of electro-weak symmetry breaking. II. The Higgs bosons in the minimal supersymmetric model*, *Phys. Rept.* **459** (2008) 1–241, [[hep-ph/0503173](#)].

- [35] B. Grinstein and M. B. Wise, *Weak Radiative B Meson Decay as a Probe of the Higgs Sector*, *Phys. Lett. B* **201** (1988) 274–278.
- [36] W.-S. Hou and R. Willey, *Effects of Extended Higgs Sector on Loop Induced B Decays*, *Nucl. Phys. B* **326** (1989) 54–72.
- [37] B. Grinstein, R. P. Springer and M. B. Wise, *Strong Interaction Effects in Weak Radiative \bar{B} Meson Decay*, *Nucl. Phys. B* **339** (1990) 269–309.
- [38] A. Buras, M. Misiak, M. Munz and S. Pokorski, *Theoretical uncertainties and phenomenological aspects of $B \rightarrow X(s)$ gamma decay*, *Nucl. Phys. B* **424** (1994) 374–398, [hep-ph/9311345].
- [39] P. Ciafaloni, A. Romanino and A. Strumia, *Two loop QCD corrections to charged Higgs mediated $b \rightarrow s$ gamma decay*, *Nucl. Phys. B* **524** (1998) 361–376, [hep-ph/9710312].
- [40] C. Bobeth, M. Misiak and J. Urban, *Matching conditions for $b \rightarrow s\gamma$ and $b \rightarrow sg$ in extensions of the standard model*, *Nucl. Phys. B* **567** (2000) 153–185, [hep-ph/9904413].
- [41] C. Bobeth, M. Misiak and J. Urban, *Photonic penguins at two loops and m_t dependence of $BR[B \rightarrow X_s l^+ l^-]$* , *Nucl. Phys. B* **574** (2000) 291–330, [hep-ph/9910220].
- [42] P. Gambino and M. Misiak, *Quark mass effects in anti- $B \rightarrow X(s)$ gamma*, *Nucl. Phys. B* **611** (2001) 338–366, [hep-ph/0104034].
- [43] K. Cheung and O. C. Kong, *Can the two Higgs doublet model survive the constraint from the muon anomalous magnetic moment as suggested?*, *Phys. Rev. D* **68** (2003) 053003, [hep-ph/0302111].
- [44] M. Misiak and M. Steinhauser, *Three loop matching of the dipole operators for $b \rightarrow s\gamma$ and $b \rightarrow sg$* , *Nucl. Phys. B* **683** (2004) 277–305, [hep-ph/0401041].
- [45] M. Czakon, U. Haisch and M. Misiak, *Four-Loop Anomalous Dimensions for Radiative Flavour-Changing Decays*, *JHEP* **03** (2007) 008, [hep-ph/0612329].
- [46] M. Misiak et al., *Updated NNLO QCD predictions for the weak radiative B-meson decays*, *Phys. Rev. Lett.* **114** (2015) 221801, [1503.01789].
- [47] M. Misiak and M. Steinhauser, *Weak radiative decays of the B meson and bounds on M_{H^\pm} in the Two-Higgs-Doublet Model*, *Eur. Phys. J. C* **77** (2017) 201, [1702.04571].
- [48] M. Misiak, A. Rehman and M. Steinhauser, *Towards $\bar{B} \rightarrow X_s \gamma$ at the NNLO in QCD without interpolation in m_c* , *JHEP* **06** (2020) 175, [2002.01548].

- [49] A. G. Akeroyd, S. Moretti, K. Yagyu and E. Yildirim, *Light charged Higgs boson scenario in 3-Higgs doublet models*, *Int. J. Mod. Phys. A* **32** (2017) 1750145, [1605.05881].
- [50] T. Inami and C. S. Lim, *Effects of Superheavy Quarks and Leptons in Low-Energy Weak Processes $k(L) \rightarrow \mu \text{ anti-}\mu$, $K^+ \rightarrow \pi^+ \text{ Neutrino anti-neutrino}$ and $K^0 \leftrightarrow \text{anti-}K^0$* , *Prog. Theor. Phys.* **65** (1981) 297.
- [51] M. Misiak and M. Steinhauser, *NNLO QCD corrections to the anti- $B \rightarrow X(s)$ gamma matrix elements using interpolation in $m(c)$* , *Nucl. Phys. B* **764** (2007) 62–82, [hep-ph/0609241].
- [52] S. M. Barr and A. Zee, *Electric Dipole Moment of the Electron and of the Neutron*, *Phys. Rev. Lett.* **65** (1990) 21–24.
- [53] A. Pilaftsis, *Higgs mediated electric dipole moments in the MSSM: An application to baryogenesis and Higgs searches*, *Nucl. Phys. B* **644** (2002) 263–289, [hep-ph/0207277].
- [54] ACME collaboration, V. Andreev et al., *Improved limit on the electric dipole moment of the electron*, *Nature* **562** (2018) 355–360.
- [55] T. S. Roussy et al., *An improved bound on the electron’s electric dipole moment*, *Science* **381** (2023) adg4084, [2212.11841].
- [56] K. Hagiwara, R. D. Peccei, D. Zeppenfeld and K. Hikasa, *Probing the Weak Boson Sector in $e^+ e^- \rightarrow W^+ W^-$* , *Nucl. Phys. B* **282** (1987) 253–307.
- [57] ATLAS collaboration, M. Aaboud et al., *Measurement of $WW/WZ \rightarrow \ell\nu qq'$ production with the hadronically decaying boson reconstructed as one or two jets in pp collisions at $\sqrt{s} = 8 \text{ TeV}$ with ATLAS, and constraints on anomalous gauge couplings*, *Eur. Phys. J. C* **77** (2017) 563, [1706.01702].
- [58] CMS collaboration, A. M. Sirunyan et al., *Search for anomalous triple gauge couplings in WW and WZ production in lepton + jet events in proton-proton collisions at $\sqrt{s} = 13 \text{ TeV}$* , *JHEP* **12** (2019) 062, [1907.08354].
- [59] CMS collaboration, A. M. Sirunyan et al., *Measurements of $pp \rightarrow ZZ$ production cross sections and constraints on anomalous triple gauge couplings at $\sqrt{s} = 13 \text{ TeV}$* , *Eur. Phys. J. C* **81** (2021) 200, [2009.01186].
- [60] B. Grzadkowski, O. M. Ogreid and P. Osland, *CP-Violation in the ZZZ and ZWW vertices at e^+e^- colliders in Two-Higgs-Doublet Models*, *JHEP* **05** (2016) 025, [1603.01388].
- [61] H. E. Haber, V. Keus and R. Santos, *P-even, CP-violating signals in scalar-mediated processes*, *Phys. Rev. D* **106** (2022) 095038, [2206.09643].

- [62] J. L. Feng, I. Galon, F. Kling and S. Trojanowski, *ForwArd Search ExpeRiment at the LHC*, *Phys. Rev. D* **97** (2018) 035001, [1708.09389].
- [63] P. Drechsel, G. Moortgat-Pick and G. Weiglein, *Prospects for direct searches for light Higgs bosons at the ILC with 250 GeV*, *Eur. Phys. J. C* **80** (2020) 922, [1801.09662].
- [64] F. Kling, S. Li, H. Song, S. Su and W. Su, *Light Scalars at FASER*, *JHEP* **08** (2023) 001, [2212.06186].
- [65] T. Robens, *A short overview on low mass scalars at future lepton colliders – LCWS23 proceedings*, in *International Workshop on Future Linear Colliders*, 7, 2023. 2307.15962.
- [66] CMS collaboration, A. M. Sirunyan et al., *Search for a standard model-like Higgs boson in the mass range between 70 and 110 GeV in the diphoton final state in proton-proton collisions at $\sqrt{s} = 8$ and 13 TeV*, *Phys. Lett. B* **793** (2019) 320–347, [1811.08459].
- [67] T. Biekötter, M. Chakraborti and S. Heinemeyer, *A 96 GeV Higgs boson in the N2HDM*, *Eur. Phys. J. C* **80** (2020) 2, [1903.11661].
- [68] S. Heinemeyer, C. Li, F. Lika, G. Moortgat-Pick and S. Paasch, *A 96 GeV Higgs Boson in the 2HDMS: e^+e^- collider prospects*, in *International Workshop on Future Linear Colliders*, 5, 2021. 2105.11189.
- [69] S. Heinemeyer, C. Li, F. Lika, G. Moortgat-Pick and S. Paasch, *Phenomenology of a 96 GeV Higgs boson in the 2HDM with an additional singlet*, *Phys. Rev. D* **106** (2022) 075003, [2112.11958].
- [70] T. Biekötter, S. Heinemeyer and G. Weiglein, *Mounting evidence for a 95 GeV Higgs boson*, *JHEP* **08** (2022) 201, [2203.13180].
- [71] T. Biekötter, S. Heinemeyer and G. Weiglein, *Excesses in the low-mass Higgs-boson search and the W-boson mass measurement*, *Eur. Phys. J. C* **83** (2023) 450, [2204.05975].
- [72] T. Biekötter, S. Heinemeyer and G. Weiglein, *The CMS di-photon excess at 95 GeV in view of the LHC Run 2 results*, *Phys. Lett. B* **846** (2023) 138217, [2303.12018].
- [73] T. Biekötter, S. Heinemeyer and G. Weiglein, *The 95.4 GeV di-photon excess at ATLAS and CMS*, 2306.03889.
- [74] J. Cao, X. Jia, Y. Yue, H. Zhou and P. Zhu, *96 GeV diphoton excess in seesaw extensions of the natural NMSSM*, *Phys. Rev. D* **101** (2020) 055008, [1908.07206].

- [75] R. Benbrik, M. Boukidi, S. Moretti and S. Semlali, *Explaining the 96 GeV Di-photon anomaly in a generic 2HDM Type-III*, *Phys. Lett. B* **832** (2022) 137245, [2204.07470].
- [76] D. Azevedo, T. Biekötter and P. M. Ferreira, *2HDM interpretations of the CMS diphoton excess at 95 GeV*, *JHEP* **11** (2023) 017, [2305.19716].
- [77] LEP HIGGS WORKING GROUP FOR HIGGS BOSON SEARCHES, OPAL, ALEPH, DELPHI, L3 collaboration, *Search for the standard model Higgs boson at LEP*, in *2001 Europhysics Conference on High Energy Physics*, 7, 2001. hep-ex/0107029.
- [78] P. A. McNamara and S. L. Wu, *The Higgs particle in the standard model: Experimental results from LEP*, *Rept. Prog. Phys.* **65** (2002) 465–528.
- [79] CMS collaboration, A. Tumasyan et al., *Searches for additional Higgs bosons and for vector leptoquarks in $\tau\tau$ final states in proton-proton collisions at $\sqrt{s} = 13$ TeV*, *JHEP* **07** (2023) 073, [2208.02717].
- [80] S. Iguro, T. Kitahara and Y. Omura, *Scrutinizing the 95–100 GeV di-tau excess in the top associated process*, *Eur. Phys. J. C* **82** (2022) 1053, [2205.03187].
- [81] A. Crivellin and B. Mellado, *Anomalies in particle physics and their implications for physics beyond the standard model*, *Nature Rev. Phys.* **6** (2024) 294–309, [2309.03870].
- [82] ATLAS collaboration, *Search for diphoton resonances in the 66 to 110 GeV mass range using 140 fb^{-1} of 13 TeV pp collisions collected with the ATLAS detector*, tech. rep., CERN, Geneva, 2023.
- [83] ATLAS collaboration, G. Aad et al., *ATLAS searches for additional scalars and exotic Higgs boson decays with the LHC Run 2 dataset*, 2405.04914.
- [84] T. Hahn, *Routines for the diagonalization of complex matrices*, physics/0607103.